Computational Modeling of Oxygen Consumption in the Heart Based on PET Measurements

by

Fu Yan

A Thesis

Submitted to the Faculty

of

WORCESTER POLYTECHNIC INSTITUTE

in partial fulfillment of the requirements for the

Degree of Master of Science

in

Applied Mathematics

by

May 2003

APPROVED:

Professor Dalin Tang, Thesis Advisor

Professor Bogdan Vernescu, Department Head

Abstract

Many cardiovascular diseases are partly due to heart muscle malfunctions. The main dynamic function in the heart is metabolism via mitochondrial respiration. And the most direct measure of oxidative tissue metabolism is the conversion rate of oxygen to water. Finding the oxygen consumption rate in the heart vessel will help us prevent the heart diseases. In the experiment, $[^{15}O]$-labeled RBCs (Red Blood Cells) and indocyanine green dye were injected into the isolated blood-perfused rabbit heart. The dye curves defined the inflow for the dye have the same shape as the inflow curves for the $[^{15}O]$ oxygen. The inflow and outflow dilution curves for $[^{15}O]$ were obtained with use of PET (Positron Emission Tomography) technology. After appropriate correction for baseline and radioactive decay, the data were transferred to a UNIX workstation for model analysis.

A linear, three-region (capillary space, interstitial fluid space, and parenchymal cell space), and axially distributed model is introduced to simulate the oxygen consumption process and determine the oxygen conversion rate. Parameters of concentration are oxygen and water corresponding to capillary space, interstitial fluid space, and parenchymal cell space. The diffusion coefficients are largely independent of molecular motion. The blood flow happens only in capillary part. Other parameters are determined by experimental data. Using the input data, consumption rate

is determined through a process minimizing the difference between the experimental and numerical output. Effects of key parameters on oxygen concentration and consumption rate are investigated.

Acknowledgements

I would like to express my deep thanks and appreciation to my thesis advisor, Dr. Dalin Tang, for his help and support. Dr. Tang helped me to keep focused on long term goals and make progress toward the completion of my work. With his encouragement, I was able to overcome all the difficulties in my research and complete this project successfully.

My thanks also go to Mathematical Sciences Department, all the faculty and staff. I would like to thank Prof. Homer Walker, Prof. Roger Lui, Prof. Mayer Humi, Prof. Jung-Han Kimn for teaching me and for their advice.

I also would like to thank all the TAs in Mathematical Science Department for giving me a happy and comfortable study atmosphere.

Many thanks to my husband Guangsen Tian for moral support and for having an open ear every time I needed someone to listen.

Contents

List of Figures

List of Tables

Chapter 1

Introduction

At present there are many diseases related to heart vessels such as coronary heart disease, heart attack, high blood pressure, cardiac arrhythmias, sudden cardiac death, heart valve disease, congenital heart defects, stroke [15]. These diseases are partly due to the malfunction of heart muscle. In other words the heart muscle does not get enough oxygen, a condition called myocardial ischemia. There are some methods to diagnose diseases, for example electrocardiographic monitor (ECG machine). But the ECG monitor shows whether the heart muscle is getting enough blood. It can not tell further information about the function of the heart muscle. Especially in the early stage of diseases blood flow changes subtly. Very often, a heart attack occurs without warning; indeed many people who suffer heart attacks are unaware that they have diseased coronary arteries until they are stricken [14]. The predominant source of energy production in the heart is oxidative metabolism, which even prevails under conditions of restricted blood flow [27]. Through measuring the conversion rate of oxygen to water we can predict the heart diseases. The importance of oxidative metabolism for intact myocardial function is emphasized by the rapid decrease of phosphocreatine levels and the concomitant increase of cardiac diameter during oxygen deprivation [10].

Although the classical view is that the normal heart flow and function are homogeneously distributed, even under physiological conditions coronary perfusion exhibits a high degree of regional heterogeneity [2]. So the analysis of the oxygen consumption is regional. Positron emission tomography (PET) or nuclear magnetic resonance (NMR) are used to measure oxygen tracer concentration in the heart. But the accuracy of the methods has not been assessed. In one word the most direct measure of oxidative tissue metabolism is the conversion rate of oxygen to water via mitochondrial respiration. One can calculate the oxygen consumption from the analysis of tissue residue curves or outflow dilution curves acquired by PET or NMR technology [10].

Compartment means that the amount of material that acts as though it is well-mixed and kinetically homogeneous. A compartmental model is a model consisting of a finite number of compartments with specific interconnections among the compartments. The interconnections represent a flux of material which physiologically represents transport from one location to another, chemical transformation, or both.

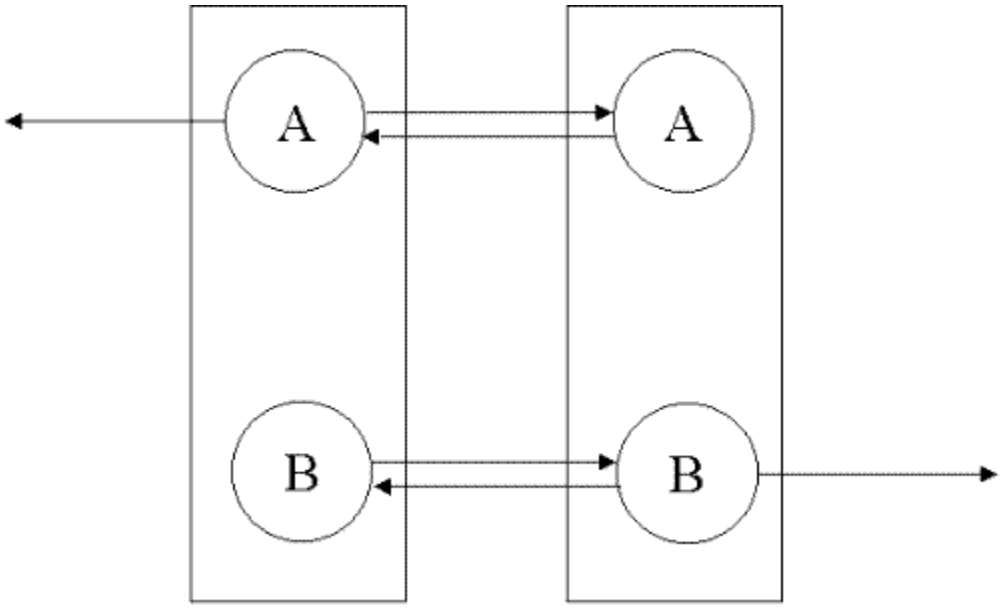

Figure 1.1: A picture of a compartmental model

Fig. 1.1 helps us define what compartments are. The figure shows two substances, A and B. Both exist in plasma (left box) and liver (right box). Thus, the plasma concentration of A and the plasma concentration of B are both represented as compartments (closed circles); the liver concentration of A and the liver concentration of B are also compartments. While A can be irreversibly lost from plasma, no exchange in plasma can occur between A and B; this exchange occurs in the liver. Both A and B can exchange between plasma and liver, and B can be lost (metabolized) in the liver, but not in plasma [8].

But there is shortcoming for this model. Compartmental models most widely used in the analysis of PET data do not consider the possible effects of longitudinal(axial) diffusion gradients along the capillary length and the effects of low heterogeneity. Furthermore, the applicability of compartmental analysis to high-temporal resolution data is limited [10].

Napper created a mathematical model of oxygen transport and consumption in the isolated-perfused heart which was developed, based on data from an auto regulating, cell-free perfused, externally paced, isovolumic feline heart preparation. The model features the unique combination of Michaelis-Menten kinetics, and one-dimensional (axial) diffusion in radially well-mixed tissue. An adaptive finite-difference integration routine was used to solve the resulting third order stiff two-point boundary value problem [30].

Groebe's model is described as below. A model of combined convective and diffusive O_2 transport to tissue is suggested which allows for the calculation of PO_2 distributions in a cuboid tissue region with arbitrary micro-vascular geometries and blood flows. Carrier-facilitated O_2 diffusion in the erythrocytes and in the tissue and red blood cell reaction kinetics are considered. The model is based on analytical descriptions of the PO_2 fields of single erythrocytes surrounded by carrier-free layers in

an infinite three-dimensional space containing an O_2 carrier such as myoglobin. These PO_2 fields are overlaid to obtain a solution of the differential equation of diffusion in respiring tissue [17].

The relatively sophisticated distributed models of Groebe and Thews, Napper and Schubert, and Popel mainly target oxygen transport in a steady state on the cellular and sub-cellular level, and their solutions are not suited for the analysis of tracer transients [10].

The oxygen model used by Rose and Goresky for studies using $[^{18}O]$oxygen measured by mass spectrometry has been the best available for analyzing transients in oxygen consumption; $[^{18}O]$water, however, the product of the reaction, is not distinguishable from background $[^{18}O]$water and was not included in the model.

Theoretical models of oxygen transport in the myocardium have failed to account for low average tissue PO_2 relative to coronary sinus PO_2, measured with PO_2 electrodes and myoglobin saturation, and for hypoxia contractile failure at relatively high coronary sinus PO_2 levels. These findings could be explained by either arteriovenous diffusional shunting or a limiting rate of transfer of oxygen from blood to tissue, or both. To gain new insights, we performed multiple indicator dilution tracer experiments across the coronary circulation in the dog, with $^{18}O_2$ as the oxygen tracer and 51Cr-labeled red cells as the reference tracer for oxygen. 125I-Albumin and 22Na+ were included to provide the relative plasma flow rate. The tracer oxygen outflow curve consisted of a large early peak related to its reference red cell curve. No tracer emerged before the labeled red cells. The downslope, which contains the returning component of the tracer curve, decreased less steeply when oxygen consumption was reduced by propranolol. Fitting the tracer oxygen outflow curve with a distributed model including irreversible sequestration behind a resistance gave a transfer rate constant which was relatively small, and a relatively large rate constant for sequestration.

Relative oxygen consumption (estimated from the arteriovenous difference) correlated closely with the rate constant for sequestration. Estimated average tissue oxygen concentrations were of the order of one-third blood concentration. Dimensional analysis indicates that the low transfer rate constant derives from hemoglobin-oxygen binding; this decreases fractional tracer oxygen transfer in proportion to the ratio of plasma: red cell oxygen pools [29].

Oxygen transport from capillaries to exercising skeletal muscle is studied by use of a Krogh-type cylinder model. The goal is to predict oxygen consumption under conditions of high demand, on the basis of a consideration of transport processes occurring at the microvascular level. Effects of the decline in oxygen content of blood flowing along capillaries, intra-vascular resistance to oxygen diffusion, and myoglobin-facilitated diffusion are included. Parameter values are based on human skeletal muscle. The dependence of oxygen consumption on oxygen demand, perfusion, and capillary density are examined. When demand is moderate, the tissue is well oxygenated and consumption is slightly less than demand. When demand is high, capillary oxygen content declines rapidly with axial distance and radial oxygen transport is limited by diffusion resistance within the capillary and the tissue. Under these conditions, much of the tissue is hypoxia, consumption is substantially less than demand, and consumption is strongly dependent on capillary density. Predicted consumption rates are comparable with experimentally observed maximal rates of oxygen consumption [23].

Chapter 2

PET Technology

2.1 Overview

PET (Positron Emission Tomography) is a nuclear medicine procedure that produces pictures of the body's biological functions. Developed in the early 1970s, PET is rapidly emerging from halls of research and academic centers into everyday clinical practice. PET provides the means for imaging the rates of biologic processes in vivo. Imaging is accomplished through the integration of two technologies, the tracer kinetic assay method and computed tomography (CT). The tracer kinetic assay method employs a radio-labeled biologically active compound (tracer) and a mathematical model that describes the kinetics of the tracer as it participates in a biological process. The tissue tracer concentration measurement required by the tracer kinetic model is provided by the PET scanner, with the final result being a three dimensional image of the anatomic distribution of the biological process under study [22].

2.2 Benefits of PET Exams

- Monitors therapeutic efficiency

  PET manages patient therapy by monitoring response to a given regimen and providing early feedback on its efficacy . This can help avoid ineffective treatments or unnecessary hospitalization.

- Identifies distant metastases

  Through showing all the organs of the body with one image, PET can identify distant, occult metastases that may affect the course of treatment and therefore change patient management.

- Eliminates invasive procedures

  PET helps avoid the expense and pain of removing benign nodules, as well as invasive biopsy procedures to determine malignancy.

- Pre-surgical assessment

  PET allows for more accurate staging of patients for surgery. Thus eliminating those procedures that will not benefit the patient and ultimately avoiding useless surgical resections.

- Earlier diagnosis

  PET is able to diagnose disease before structural changes become detectable with anatomical imaging techniques, potentially improving the prognosis [1].

2.3 Applications in PET

- Oncology

In oncology, PET is the only modality that can accurately image many organs of the body with a single pass to allow determination of malignancy. It can also provide information to determination of whether a primary cancer has metastasized to other parts of the body. PET has demonstrated its usefulness in: cost effective, whole-body metastatic surveys; avoiding biopsies for low-grade tumors; non-invasive differentiation of tumors from radiation necrosis; early change in course of ineffective chemotherapy; and avoiding unnecessary diagnostic and therapeutic surgeries. PET is effective in the diagnosing and staging of the following cancers: brain tumor, breast cancer, colorectal cancer, head and neck cancer, lung cancer and so on.

- Cardiology

  In cardiology, PET enables physicians to screen for coronary artery disease, to assess flow rates and flow reserve, and to distinguish viable from nonviable myocardium for bypass and transplant candidates.

- Neurology

  In neurology, PET provides information for assessing various neurological diseases such as Alzheimer's and other dementias, Parkinson's, and Huntington's. Additionally, it localize epileptic foci's for qualifying and identifying the site for surgical intervention. It allows the characterization, grading, and assessment of possible brain tumor recurrence. In neurological cases, PET is also used for evaluation of stroke and epilepsy [24].

2.4 Basic principle of PET

In clinical applications, a very small amount of labeled compound (called radio-pharmaceutical or radio-tracer) is introduced into the patient usually by intravenous

injection and after an appropriate uptake period, the concentration of tracer in tissue is measured by the scanner. During its decay process,the radionuclide emits a positron which, after traveling a short distance (3-5 mm), encounters an electron from the surrounding environment. The two particles combine and "annihilate" each other resulting in the emission in opposite directions of two gamma rays. The image acquisition is based on the external detection in coincidence of the emitted γ-rays, and a valid annihilation event requires a coincidence within 12 nanoseconds between two detectors on opposite sides of the scanner. For accepted coincidences, lines of response connecting the coincidence detectors are drawn through the object and used in the image reconstruction. Any scanner requires that the radioisotope, in the field of view, does not redistribute during the scan. A tissue attenuation correction is performed by recording a short transmission scan using γ-rays from three radioactive (Germanium-68/Gallium-68) rotating rod sources [25].

2.5 PET Applied in Cardiology

The application is for the assessment of regional oxidative metabolism in vivo from tissue ^{15}O-residue curves obtained by PET.

The imaging system is a General Electric Advance whole body positron emission tomography providing 35 image planes of data over a 15 cm axial field of view. The system at the University of Washington is configured with a 20 i860 cpu array processor providing reconstruction times of 1 second per image for 2D data sets and 6.8 seconds per image for 3D data sets. The system includes two HP735 workstations for scanner control and image display.

Chapter 3

The Background to Blood-Tissue Exchange Model

We study blood flow in heart muscle with oxygen consumption which requires background study for fluid flow in a pipe, conservation and transfer of mass (blood carrying oxygen), two-phase flow (blood and oxygen carrying ^{15}O or blood and water carrying ^{15}O), diffusion and conduction. In this chapter we review the needed material and related differential equation knowledge.

There has been a gradual development of blood-tissue exchange models since Christian Bohr showed that the concentration of a solute escaping from a long capillary should diminish exponentially as a function of the distance along the tube. Given that radial diffusion inside and outside of the capillary is rapid, and that the return flux is negligible, the extraction occurring between inflow and outflow is given by:

$$E = 1 - e^{-PS_C/F_S} \tag{3.1}$$

where E is an extraction, PS_C is the capillary permeability-surface area product, and F_S is the flow of solute-containing fluid, i.e., plasma or whole blood. Although the model represented by Eq3.1 was useful, and allowed the estimation of capillary permeabilities for the first time, it is incomplete since it does not conserve mass. Newer

models defined by James B. Bassingthwaighte are mass conservative, and not only allow testing of the adequacy of Eq3.1, but extend the power of the multiple indicator dilution approach to estimating cellular parameters of the system, cell membrane transport, and intracellular reaction rates [5]. Our model is base on the model defined by James B. Bassingthwaighte. At the same time we consider mass transfer. The detail will be introduced in chapter 4. I introduce basic knowledge about conservation and transfer of mass in the below section.

3.1 Conservation and Transfer of Mass

3.1.1 Conservation of Mass

For each time t, we shall assume that the fluid has a well-defined mass density $\rho(x,t)$. Thus if W is any subregion of D, we assume that the mass of fluid in W at time t is given by

$$m(W,t) = \int_W \rho(x,t)dV(t) \tag{3.2}$$

where dV is the volume element in the plane or in space.

Conservation of mass is based on that mass is neither created nor destroyed.

The rate of change of mass in W is

$$\frac{d}{dt}m(W,t) = \frac{d}{dt}\int_W \rho(x,t)dV(x) \tag{3.3}$$

$$= \int_W \frac{\partial \rho}{\partial t}(x,t)dV(x) \tag{3.4}$$

Let ∂W denote the boundary of W, assumed to be smooth, let n denote the unit outward normal defined at points of ∂W, and let dA denote the area element on ∂W. The volume flow rate across ∂W per unit area is $u \cdot n$ and the mass flow rate per unit area is $\rho u \cdot n$.

The principle of conservation of mass can be more precisely stated as: the rate of change of mass in W equals the rate at which mass is crossing ∂W in the inward direction; i.e.

$$\frac{d}{dt}\int_W \rho dV = -\int_{\partial W} \rho u \cdot n dA \tag{3.5}$$

This is the integral form of the law of conservation of mass. By the divergence theorem, this statement is equivalent to

$$\int_W (\frac{\partial \rho}{\partial t} + div(\rho u))dV = 0 \tag{3.6}$$

Since this is to hold for all W, it is equivalent to

$$\frac{\partial \rho}{\partial t} + div(\rho u) = 0 \tag{3.7}$$

The last equation is the differential form of the law of conservation of mass, also known as the continuity equation [7].

In our model we are based not only on conservation of mass but also on transfer of mass.

3.1.2 Transfer of Mass

In our case oxygen converts to water when metabolism happens. In this procedure transfer of mass takes place. Here we make assumption that all oxygen and water are well mixed, except near the oxygen-water interface since it makes easy that we analyze the mass transfer coefficients.

We expect that the amount transferred is proportional to the concentration difference and the interfacial area:

$$\big(\text{amount of mass transferred }\big) = k\big(\text{interfacial area}\big)\big(\text{concentration difference}\big)$$

where the proportionality is summarized by k, called a mass transfer coefficient. If we divide both side of this equation by the area, we can write the equation in more familiar symbols:

$$N_1 = k(C_2 - C1) \tag{3.8}$$

where N_1 is the flux at the interface and C_2 and C_1 are the concentrations at the interface and in the bulk solution, respectively. We introduce this definition with the implication that it provides a simple way of analyzing complex problems. We imply that the mass transfer coefficient has funtions as the density or the viscosity, a physical quantity that is well defined for a specific situation.

In fact there are a variety of definitions of mass transfer coefficients. This variety is largely an experimental artifact, arising because the concentration can be measured in many different units, including partial pressure, mole and mass fractions, and molarity.

The common equation for gas absorption is as below:

$$N_1 = k^{'} \triangle \rho \tag{3.9}$$

where for a gas of constant molar concentration C, $k = RTk^{'}$, ρ is the solution density.

We assume that if the flux is in moles per area per time, then the concentration difference is expressed as moles per volume. If the flux is in mass per area per time, then the concentration is given as mass per volume. Thus our mass transfer coefficient has dimensions of velocity.

We also should consider two-phase flow because blood and RBCs are well mixed in the vessel.

3.2 Introduction to Two-Phase Flow

A phase is simply one of the states of matter and can be either a gas, a liquid, or a solid. Multiphase flow is the simultaneous flow of several phases. Two-phase flow is the simplest case of multiphase flow. Blood is composed of a solid, cellular portion, called "formed elements", and a fluid portion, called "plasma". The solid elements are suspended and carried in the plasma, which contains many different types of proteins and water-solube molecules. The most import cellular elements found in blood are red blood cells (erythrocytes), white blood cells (leukocytes), and platelets. Red blood cells transport oxygen and carbon dioxide. Because we deal with metabolism, we only consider plasma-RBC (red blood cell) model. It flows obey all of the basic laws of fluid mechanics. The equations are merely more complicated or more numerous than those of single-phase flows. There are some models related to two-phase flow as shown below [33]:

- Separated flow:

  -phases considered artificially segregated (need to model interaction between the phases)

- Homogeneous flow:

  -flow assumed as equivalent single-phase flow with pseudo properties

- Drift flux:

  -"separated" flow model in which attention is focused on relative motion between phases

- Flow pattern models:

-phases considered to be arranged in one of three or four definition prescribed geometries (based on observations of configuration of phases)

Plasma and RBCs have different properties. So our model belongs to separated flow category. This kind of model may be developed with various degrees of complexity. In our case, separate equations of continuity, momentum, and energy are written for each phase and each layer and these six equations are solved simultaneously. At the same time we consider the interaction between oxygen and water (conversion rate) in six equations.

We consider three important aspects in our model shown as below:

- (1) The large number of relevant physical properties involved. Our model is mainly based on mass conservation, mass transfer and convection.
- (2) The characterization of the interface. Oxygen conversion to water happens only in the parenchymal cell space. The conversion rate is a very important parameter we need consider. Besides this point, different layers have different conductances. PS_{cap} is the conductance between capillary space and interstitial space; PS_{pc} is the conductance between interstitial space and parenchymal space.
- (3) The presence of non-equilibrium effects. The activity or chemical potential for oxygen, equivalent to its partial pressure, in accord with the principle that gradients in partial pressure provide the driving forces for the fluxes.

3.3 Diffusion and Convection

In heart muscle we consider three layers (capillary space, interstitial fluid space and parenchymal cell space). Oxygen and water are transported from capillary space

to the other two spaces. So diffusion must be considered. I introduce the fundamental concepts of diffusion as following.

3.3.1 Concepts of Diffusion

Diffusion is the process by which matter is transported from one part of a system to another as a result of random molecular motions. Fick first put diffusion on a quantitative basis by adopting the mathematical equation of heat conduction derived some years earlier by Fourier. The mathematical theory of diffusion in isotropic substances is therefore based on the hypothesis that the rate of transfer of diffusing substance through unit area of a section is proportional to the concentration gradient measured normal to the section, i.e.

$$F = -D\frac{\partial C}{\partial x} \tag{3.10}$$

where F is the rate of transfer per unit area of section, C the concentration of diffusing substance, x the space coordinate measured normal to the section, and D is called the diffusion coefficient. D is constant, independent of F and C and has dimensions $(length)^2(time)^{-1}$. The negative sign arises because diffusion occurs in the direction opposite to that of increasing concentration. The fundamental differential equation of diffusion in an isotropic medium is as below:

$$\frac{\partial C}{\partial t} + \frac{\partial F_x}{\partial x} + \frac{\partial F_y}{\partial y} + \frac{\partial F_z}{\partial z} = 0 \tag{3.11}$$

If the diffusion coefficient is constant. (3.10) and (3.11) become

$$\frac{\partial C}{\partial t} = D(\frac{\partial^2 C}{\partial x^2} + \frac{\partial^2 C}{\partial y^2} + \frac{\partial^2 C}{\partial z^2}) \tag{3.12}$$

reducing simply to

$$\frac{\partial C}{\partial t} = D\frac{\partial^2 C}{\partial x^2} \tag{3.13}$$

If diffusion is one-dimensional i.e. if there is a gradient of concentration only along the x-axis [9]. But we must consider the rate of creation per unit volume. So the above equation is transfered to:

$$\frac{\partial C}{\partial t} = D\frac{\partial^2 C}{\partial x^2} + A \tag{3.14}$$

3.3.2 Convection Effects

Diffusion causes convection. It occurs because of concentration differences in our case. In more modern terms, we would say that any mass flux may include both convection and diffusion. But when we analyze dilute solutions, we can consider the convection caused by diffusion is vanishingly small. This dilute limit provides the framework within which most people analyze diffusion.

General equation for mass balance is shown as below:

$$\frac{\partial C}{\partial t} + v_x\frac{\partial C}{\partial x} + v_y\frac{\partial C}{\partial y} + v_z\frac{\partial C}{\partial z} = D(\frac{\partial^2 C}{\partial x^2} + \frac{\partial^2 C}{\partial y^2} + \frac{\partial^2 C}{\partial z^2}) + r \tag{3.15}$$

Our case is one dimensional situation since metabolism happens in a very thin vessel.

$$\frac{\partial C}{\partial t} + v_x\frac{\partial C}{\partial x} = D\frac{\partial^2 C}{\partial x^2} + r \tag{3.16}$$

The diffusion coefficient D is assumed constant. The conductance coefficient r is the rate of production per volume. Because we take into account convection of oxygen and water flow, the concentration flux at the surface is the product of the conductance and a concentration potential difference.

$$\frac{\partial C_1}{\partial t} = PS(C_1 - C_2) \tag{3.17}$$

Next chapter our mathematical model is introduced in detail.

Chapter 4

Mathematical Model

A mathematical model to simulate the oxygen consumption in heart muscle is developed in this chapter, which accounts for diffusion, convection and transformation in the tissue. Firstly a linear three-region axially distributed model and the purpose of the model are introduced in this chapter. Based on the model all kinds of parameters, partial differential equations, and boundary and initial conditions are provided. And then the experimental procedure is briefly given in order to give an idea of how to achieve the mathematical model in practical operation.

4.1 Three-Region Axially Distributed Model

The model consists of three layers, which are capillary space, interstitial fluid space and parenchymal cell space. It summarizes blood-tissue exchange of $[^{15}O]$oxygen, metabolism to form $[^{15}O]$water, and tissue-blood exchange of tracer water. There are two three-region models in parallel, for oxygen and water, with the transformation occurring only in parenchymal cells governed by the gulosity (consumption) term G_{pc}. The detail is shown in Figure 4.1 [10].

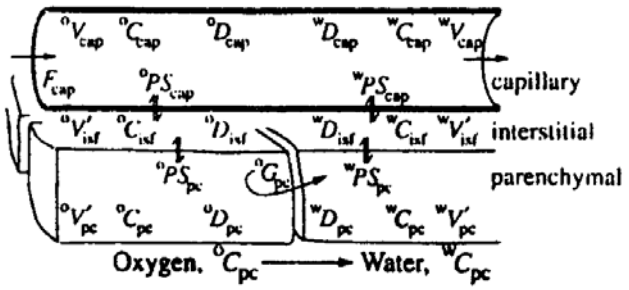

Figure 4.1: Three-region axially distributed model

Blood flows in the capillary vessel. Oxygen carried by blood penetrates (through diffusion and conductance) interstitial space and parenchymal space where part of oxygen consumption takes place. When oxygen is consumed, it becomes water (one oxygen atom takes two hydrogen atoms). The model obeys the law of conservation of mass, thus consumption of oxygen is coupled with the formation of an equivalent amount of water ($1/2O_2 \rightarrow H_2O$). For $[^{15}O]$oxygen, only one oxygen atom in each oxygen molecule is labeled; the ^{15}O-labeled oxygen is really $^{15}O^{16}O$. Hence, for the present application, the disappearance of one oxygen label results in the generation of one water label [10].

By using tracer $[^{15}O]$ and PET (Positron Emission Tomography) technology, the amount of $[^{15}O]$ that enters the system (input) and the amount of residue (part of $[^{15}O]$ and water) that exits the system (output) can be measured. Based on the input and output data, our job is to introduce mathematical models to calculate the oxygen consumption rate which can not be measured directly.

This model is linear and is therefore suited for the analysis of tracer fluxes in a system in steady state with respect to local oxygen partial pressures. The model
1) permits the physiologically realistic description of oxygen transport and conversion into water for tracer transients as well as for steady-state mother substrate with the

use of a single parameter set that governs the kinetics of both tracer and mother substance, 2) takes the regional heterogeneity of flow and metabolism into account, 3) has an anatomically appropriate structure and provides time-domain solutions that can be fitted to residue data as well as to outflow data to provide estimates of the parameters for transport and consumption [10].

In order to get the solution of this model, we made several reasonable assumptions.

1) Large vessel and capillary hematocrits are considered identical. This allows us to consider that RBC and plasma velocities are equal. Although this assumption is not quite correct, because erythrocyte mean transit times through the coronary system are a few percent less than plasma transit times, it results in little error; most of the O_2 in the blood is in the erythrocyte and is accounted for via the volume of distribution ${}^{o}V_{cap}$, which is the anatomic volume, so the convective velocity is correct.

2) Exchange occurs only in the capillary-tissue exchange unit, not in the arterioles or venules.

3) Within the capillary, oxygen in erythrocytes and plasma are in continuous equilibrium. This assumption is not quite correct when oxygen is being consumed but introduces almost no error because the plasma oxygen content is low compared with that in the erythrocyte. The resistance to oxygen flux from RBC to plasma is therefore accounted for as part of ${}^{o}PS_{cap}$ [10].

Based on these consumptions partial differential equations are provided and variables and parameters are introduced.

4.2 Introduction to Variables and Parameters

Because the model is related to oxygen and water in RBCs, the number of variables and parameters is doubled. At the same time there are three regions representing capillary space (cap), interstitial fluid space (isf), and parenchymal cell space (pc) in our model, that again triples the number of variables and parameters. In order to establish mathematical equations conveniently we introduce unknown variables and suitable parameters firstly.

4.2.1 Variables Used in the Oxygen Consumption Model

The overall variable is concentration. But because we need to consider two-phase flow and three regions, there should be 6 variables totally. They are functions of time (t) and space (x). They are listed as: ${}^{o}C_{cap}, {}^{o}C_{isf}, {}^{o}C_{pc}, {}^{w}C_{cap}, {}^{w}C_{isf}, {}^{w}C_{pc}$.

Their meanings are shown as below:

${}^{o}C_{cap}$ represents oxygen concentration in capillary space;

${}^{o}C_{isf}$ represents oxygen concentration in interstitial space;

${}^{o}C_{pc}$ represents oxygen concentration in parenchymal space;

${}^{w}C_{cap}$ represents water concentration in capillary space;

${}^{w}C_{isf}$ represents water concentration in interstitial space;

${}^{w}C_{pc}$ represents water concentration in parenchymal space.

4.2.2 Parameters Used in the Oxygen Consumption Model

In blood flow we need to consider parameters including oxygen consumption rate, diffusion coefficients, conductances, velocity and volumes.

In all of parameters calculating oxygen consumption rate is our major purpose. Oxygen consumption is also called gulosity. Here we use G_{pc} to represent it. Many cardiovascular diseases are partly due to heart muscle malfuntions. The main dynamic function in the heart is metabolism via mitochondrial respiration. And the most direct measure of oxidative tissue metabolism is the conversion rate of oxygen to water (G_{pc}). Finding the oxygen consumption in the heart vessel will help us prevent the heart diseases.

As we emphasize in chapter 3 that diffusion and convection have important functions on blood vessels in hearts, here we discuss diffusion and convection coefficients in our model. Because diffusion causes convection, in order to establish brief equations we use diffusion coefficients to represent their joint functions. Considered two-phase and three-region flow, there are 6 diffusion coefficients. They are listed as ${}^{o}D_{cap}$,${}^{o}D_{isf}$,${}^{o}D_{pc}$,${}^{w}D_{cap}$,${}^{w}D_{isf}$,${}^{w}D_{pc}$.

Here their meanings are shown as below:

${}^{o}D_{cap}$ represents oxygen diffusion in capillary space;

${}^{o}D_{isf}$ represents oxygen diffusion in interstitial space;

${}^{o}D_{pc}$ represents oxygen diffusion in parenchymal space;

${}^{w}D_{cap}$ represents water diffusion in capillary space;

${}^{w}D_{isf}$ represents water diffusion in interstitial space;

${}^{w}D_{pc}$ represents water diffusion in parenchymal space.

Another important parameters are conductances. The concentration flux is the product of the conductance and a concentration potential difference. The conductance is also called mass transfer coefficient. Because conductance takes place between two barriers, there are 4 parameters (2 for oxygen; 2 for water) instead of 6. They are

${}^{o}PS_{cap}$,${}^{o}PS_{pc}$,${}^{w}PS_{cap}$,${}^{w}PS_{pc}$, whose meanings are shown as following:

${}^{o}PS_{cap}$ represents oxygen conductance between capillary space and interstial space;

${}^{o}PS_{pc}$ represents oxygen conductance between interstitial space and parenchymal space;

${}^{w}PS_{cap}$ represents water conductance between capillary space and interstial space;

${}^{w}PS_{pc}$ represents water conductance between interstitial space and parenchymal space.

Based on mass balance equations (3.16) velocity is a necessary parameter when we establish the mathematical model. Blood flows in capillary vessel. So we only consider the velocity of oxygen and water in capillary. They are ${}^{o}v$,${}^{w}v$.

Their meanings are shown as following:

${}^{o}v$ represents oxygen velocity in capillary space;

${}^{w}v$ represents water velocity in capillary space.

Each region has a distinct volume. There are 6 volume parameters according to above reason. They are ${}^{o}V_{cap}$,${}^{o}V_{isf}$,${}^{o}V_{pc}$,${}^{w}V_{cap}$,${}^{w}V_{isf}$,${}^{w}V_{pc}$.

Their meanings are shown as below:

${}^{o}V_{cap}$ represents efficient oxygen volume in capillary space;

${}^{o}V_{isf}$ represents efficient oxygen volume in interstitial space;

${}^{o}V_{pc}$ represents efficient oxygen volume in parenchymal space;

${}^{w}V_{cap}$ represents efficient water volume in capillary space;

${}^{w}V_{isf}$ represents efficient water volume in interstitial space;

${}^{w}V_{pc}$ represents efficient water volume in parenchymal space.

4.3 Partial Differential Equations

The purpose that we build mathematical model is to find oxygen consumption rate (G_{pc}) in heart vessel. The method we used is to fit curve. After assuming G_{pc}, we use numerical method (FDM) to get output of oxygen concentration ($^oC_{cap}$). Through matching the experimental curve gained from PET technology, we find optimal G_{pc} to fit curve well.

Because concentration is the function of time (t) and space (x), we get the PDE for concentration based on mass balance equation:

$$\frac{\partial C_1}{\partial t} + v_x \frac{\partial C_1}{\partial x} = D\frac{\partial^2 C_1}{\partial x^2} + PS(C_1 - C_2) \tag{4.1}$$

Because we have 6 variables ($^oC_{cap}$,$^o C_{isf}$,$^o C_{pc}$,$^w C_{cap}$,$^w C_{isf}$,$^w C_{pc}$), based on above equation we get 6 equations as shown below:

The concentrations for oxygen are given by the solutions to

$$\frac{\partial {}^oC_{cap}}{\partial t} = {}^oD_{cap}\frac{\partial^2 {}^oC_{cap}}{\partial x^2} - {}^o v\frac{\partial {}^oC_{cap}}{\partial x} - \frac{{}^oPS_{cap}}{{}^oV_{cap}}({}^oC_{cap} - {}^oC_{isf}) \tag{4.2}$$

$$\frac{\partial {}^oC_{isf}}{\partial t} = {}^oD_{isf}\frac{\partial^2 {}^oC_{isf}}{\partial x^2} - \frac{{}^oPS_{cap}}{{}^oV_{isf}}({}^oC_{isf} - {}^oC_{cap}) - \frac{{}^oPS_{pc}}{{}^oV_{isf}}({}^oC_{isf} - {}^oC_{pc}) \tag{4.3}$$

$$\frac{\partial {}^oC_{pc}}{\partial t} = {}^oD_{pc}\frac{\partial^2 {}^oC_{pc}}{\partial x^2} - \frac{{}^oPS_{pc}}{{}^oV_{pc}}({}^oC_{pc} - {}^oC_{isf}) - \frac{G_{pc}}{{}^oV_{pc}}{}^oC_{pc} \tag{4.4}$$

The concentrations for water are given by the solutions to

$$\frac{\partial {}^wC_{cap}}{\partial t} = {}^wD_{cap}\frac{\partial^2 {}^wC_{cap}}{\partial x^2} - {}^w v\frac{\partial {}^wC_{cap}}{\partial x} - \frac{{}^wPS_{cap}}{{}^wV_{cap}}({}^wC_{cap} - {}^wC_{isf}) \tag{4.5}$$

$$\frac{\partial {}^wC_{isf}}{\partial t} = {}^wD_{isf}\frac{\partial^2 {}^wC_{isf}}{\partial x^2} - \frac{{}^wPS_{cap}}{{}^wV_{isf}}({}^wC_{isf} - {}^wC_{cap}) - \frac{{}^wPS_{pc}}{{}^wV_{isf}}({}^wC_{isf} - {}^wC_{pc}) \tag{4.6}$$

$$\frac{\partial {}^wC_{pc}}{\partial t} = {}^wD_{pc}\frac{\partial^2 {}^wC_{pc}}{\partial x^2} - \frac{{}^wPS_{pc}}{{}^wV_{pc}}({}^wC_{pc} - {}^wC_{isf}) + \frac{G_{pc}}{{}^wV_{pc}}{}^oC_{pc} \tag{4.7}$$

4.4 Boundary and Initial Conditions

In order to solve PDEs mentioned in last section we need furthermore conditions. Here we provide the boundary and initial conditions suitable for above PDEs.

Initial conditions:

$$
\begin{aligned}
&{}^{o}C_{cap}(x,0) = 0, {}^{o}C_{isf}(x,0) = 0, {}^{o}C_{pc}(x,0) = 0, \\
&{}^{w}C_{cap}(x,0) = 0, {}^{w}C_{isf}(x,0) = 0, {}^{w}C_{pc}(x,0) = 0
\end{aligned} \tag{4.8}
$$

This is because at $t = 0$ no tracer oxygen is injected into vessel and no tracer water is produced.

Boundary conditions:

At the vessel inlet we use experimental inflow data as boundary condition of ${}^{o}C_{cap}$. Shown in Fig.4.2.

$$
\begin{aligned}
&{}^{o}C_{isf}(0,t) = 0, {}^{o}C_{pc}(0,t) = 0, \\
&{}^{w}C_{cap}(0,t) = 0, {}^{w}C_{isf}(0,t) = 0, {}^{w}C_{pc}(0,t) = 0.
\end{aligned} \tag{4.9}
$$

At the vessel outlet all unknown variables are free.

$$
\begin{aligned}
&\frac{d^{o}C_{cap}}{dx}|_{x=L} = 0, \frac{d^{o}C_{isf}}{dx}|_{x=L} = 0, \frac{d^{o}C_{pc}}{dx}|_{x=L} = 0, \\
&\frac{d^{w}C_{cap}}{dx}|_{x=L} = 0, \frac{d^{w}C_{isf}}{dx}|_{x=L} = 0, \frac{d^{w}C_{pc}}{dx}|_{x=L} = 0.
\end{aligned} \tag{4.10}
$$

4.5 Experimental Procedure

Experimental procedure is introduced briefly in this section. Experiments using injections of $[^{15}O]$-labeled RBCs in isolated blood-perfused rabbit hearts provided

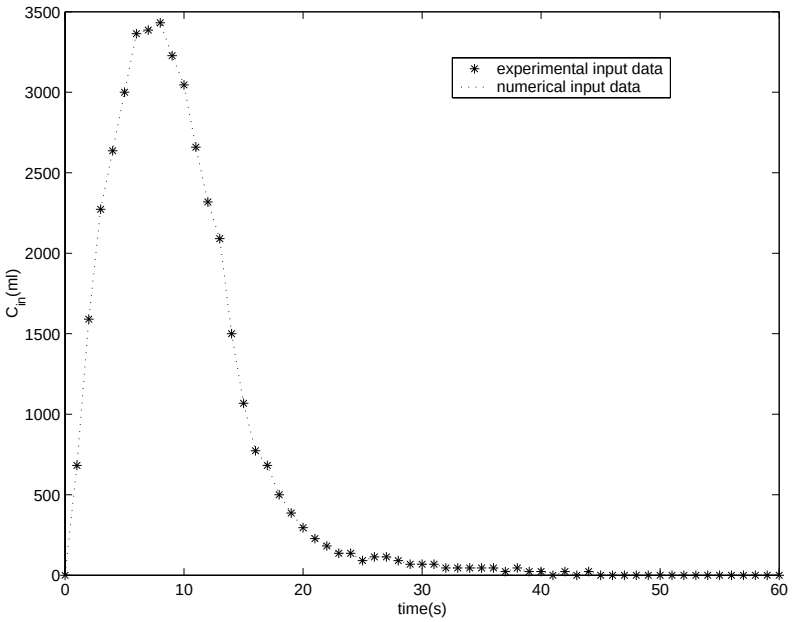

Figure 4.2: Experimental inflow data

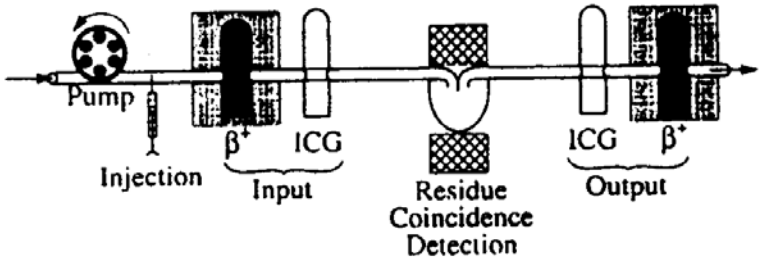

Figure 4.3: Experimental setup for isolated blood-perfused heart studies

data for testing the model for oxygen metabolism in the heart. The overall system is diagrammed in Fig.4.3.

β^+, positron-detecting plastic scintillator probes; ICG, indocyanine green detectors. NaI coincidence γ-detecting crystals are on opposite sides of heart (center) [10].

Blood of the same Hct (hematocrit) containing 20 mg/l indocyanine green dye was preequilibrated with $[^{15}O]$oxygen in an oxygenator system. This preequilibrated blood was used to fill an injection loop upstream to the heart, and the flow was switched to go through the loop to inject tracer and dye into the inflow.

Hearts were perfused at a constant flow rate with a modified Krebs-Ringer buffer containing washed human erythrocytes at a Hct of 20%, a PO_2 of 200 Torr, and a temparature of 37^oC. Coronary flow rate (typically 0.7-1.0 $ml \cdot g^{-1} \cdot min^{-1}$) was adjusted to keep coronary perfusion pressure of this "nonworking", spontaneously beating (110-130 beats/min) preparation at $50mmHg$. The coronary venous effluent perfusate exited via a catheter and advanced into the right ventricle via the pulmonary artery [10].

To obtain the transport function for the experimental setup, flow-through densitometers were placed on the coronary inflow and outflow cannular to measure the concentration time curves for indocyanine green [3]. The dye curves defined the inflow for the dye has the same shape as the inflow curves for the $[^{15}O]$ oxygen. The inflow and outflow dilution curves for $[^{15}O]$ were obtained with use of PET (Positron emission tomography) technology. The residue function of the whole heart was obtained with two thallium-activated NaI detectors used in coincidence mode and positioned to give maximal recovery of the annihilation events occurring in the heart [13]. After appropriate correction for baseline and radioactive decay, the data were transferred to a UNIX workstation for model analysis.

Chapter 5

Numerical Methods for the Model

The PDEs we got from last chapter are also called advection-diffusion-reaction equations. Unfortunately, there are only few cases for which analytical solution to the advection-diffusion-reactions exists. This fact has motivated an extensive research into numerical techniques for accurate and efficient solution of the aforesaid equations [18].

In 1953, Sangren and Sheppard [32] gave the analytical solution to a 1-barrier 2-region model, a cylindrical capillary separated by a thin barrier from a surrounding cylindrical extravascular region, in which radial diffusion was infinitely rapid and axial diffusion in both regions was zero. The model conserved mass, thus accounting for return flux from extravascular space to capillary. This model was applied by Goresky [12] to the analysis of indicator dilution curves for extracellular tracers. Bassingthwaighte [4] expressed it in numerical form, as a differential operator, using a Lagrangian approach, and accounting crudely for axial diffusion; this version was useful for analyzing sodium exchange in the heart [13]. In 1977 Rose [28] developed an "analytical" closed form solution for the analogous 2-barrier 3-region model without axial diffusion (which we call RGB77). The solution requires using series ap-

proximations (Bessel functions), the evaluation of roots of a quadratic equation and a convolution integration. Achieving accuracy is also a problem; finding the roots of a quadratic, then using them in Bessel functions, which are within a convolution integral, is not conducive to high accuracy. Lumsden and Silverman [21] extended the RGB77 expression by the minor additions of consumption terms in plasma and interstitium as well as in parenchymal cells.

Analytic solutions for 3-region capillary-tissue units with axial diffusion have not been developed, although the approach of Lenhoff and Lightfoot [20] can, in principle, be extended to do this. In our model we use backward-time central-space scheme. Reasonable mesh is created to discretize the system. Because there are 6 variables, the coefficient matrix is very complicated. Next section the coefficient matrix is given. Some numerical skills are applied.

Our numerical jobs include several steps:

- Start from an initial guess of G_{pc}.
- Use experimental input, solve the mathematical model to get numerical output.
  - Natural cubic splines method to interpolate experimental inflow data;
  - Implicit Finite difference method;
  - Backward-time, central-space scheme;
  - Backwise Gaussian Elimination method to solve systems.
- Compare numerical output with experimental output. Use Golden-Section method to adjust G_{pc} to minimize the difference between experimental data and numerical results (Least-Squares).

5.1 Discretization of the System and Numerical Method

Now we start to solve the equations (4.1-4.6) we get from chapter 4. Firstly in order to simplify equations we use another form to represent these equations.

$$\frac{\partial C_1}{\partial t} = a_1\frac{\partial^2 C_1}{\partial x^2} + b_1\frac{\partial C_1}{\partial x} + c_{11}C_1 + c_{12}C_2 \tag{5.1}$$

$$\frac{\partial C_2}{\partial t} = a_2\frac{\partial^2 C_2}{\partial x^2} + c_{21}C_1 + c_{22}C_2 + c_{23}C_3 \tag{5.2}$$

$$\frac{\partial C_3}{\partial t} = a_3\frac{\partial^2 C_3}{\partial x^2} + c_{32}C_2 + c_{33}C_3 \tag{5.3}$$

$$\frac{\partial C_4}{\partial t} = a_4\frac{\partial^2 C_4}{\partial x^2} + b_4\frac{\partial C_4}{\partial x} + c_{41}C_4 + c_{42}C_5 \tag{5.4}$$

$$\frac{\partial C_5}{\partial t} = a_5\frac{\partial^2 C_5}{\partial x^2} + c_{51}C_4 + c_{52}C_5 + c_{53}C_6 \tag{5.5}$$

$$\frac{\partial C_6}{\partial t} = a_6\frac{\partial^2 C_6}{\partial x^2} + c_{62}C_5 + c_{63}C_6 + c_{64}C_3 \tag{5.6}$$

All coefficients have meanings shown as below:

$$a_1 =^o D_{cap}, b_1 = -{}^o v, c_{11} = -\frac{{}^o PS_{cap}}{{}^o V_{cap}}, c_{12} = \frac{{}^o PS_{cap}}{{}^o V_{cap}}; \tag{5.7}$$

$$a_2 =^o D_{isf}, c_{21} = \frac{{}^o PS_{cap}}{{}^o V_{isf}}, c_{22} = -\frac{{}^o PS_{cap}}{{}^o V_{isf}} - \frac{{}^o PS_{pc}}{{}^o V_{isf}}, c_{23} = \frac{{}^o PS_{pc}}{{}^o V_{isf}}; \tag{5.8}$$

$$a_3 =^o D_{pc}, c_{32} = \frac{{}^o PS_{pc}}{{}^o V_{pc}}, c_{33} = -\frac{{}^o PS_{pc}}{{}^o V_{pc}} - \frac{G_{pc}}{{}^o V_{pc}}; \tag{5.9}$$

$$a_4 =^w D_{cap}, b_4 = -{}^w v, c_{41} = -\frac{{}^w PS_{cap}}{{}^w V_{cap}}, c_{42} = \frac{{}^w PS_{cap}}{{}^w V_{cap}}; \tag{5.10}$$

$$a_5 =^w D_{isf}, c_{51} = \frac{{}^w PS_{cap}}{{}^w V_{isf}}, c_{52} = -\frac{{}^w PS_{cap}}{{}^w V_{isf}} - \frac{{}^w PS_{pc}}{{}^w V_{isf}}, c_{53} = \frac{{}^w PS_{pc}}{{}^w V_{isf}}; \tag{5.11}$$

$$a_6 =^w D_{pc}, c_{62} = \frac{{}^w PS_{pc}}{{}^w V_{pc}}, c_{63} = -\frac{{}^w PS_{pc}}{{}^w V_{pc}}, c_{64} = \frac{G_{pc}}{{}^w V_{pc}}. \tag{5.12}$$

After using backward-time central-space scheme to equations 5.1-5.6 we get below equations:

$$A_1C_1(i-1,j+1)+B_1C_1(i,j+1)+C_{11}C_1(i+1,j+1)+C_{12}C_2(i,j+1)$$
$$=D_1C_1(i,j) \tag{5.13}$$
$$A_2C_2(i-1,j+1)+B_2C_2(i,j+1)+C_{22}C_2(i+1,j+1)+C_{21}C_1(i,j+1)$$
$$+C_{23}C_3(i,j+1)=D_2C_2(i,j) \tag{5.14}$$
$$A_3C_3(i-1,j+1)+B_3C_3(i,j+1)+C_{33}C_3(i+1,j+1)+C_{32}C_2(i,j+1)$$
$$=D_3C_3(i,j) \tag{5.15}$$
$$A_4C_4(i-1,j+1)+B_4C_4(i,j+1)+C_{44}C_4(i+1,j+1)+C_{45}C_5(i,j+1)$$
$$=D_4C_4(i,j) \tag{5.16}$$
$$A_5C_5(i-1,j+1)+B_5C_5(i,j+1)+C_{55}C_5(i+1,j+1)+C_{54}C_4(i,j+1)$$
$$+C_{56}C_6(i,j+1)=D_5C_5(i,j) \tag{5.17}$$
$$A_6C_6(i-1,j+1)+B_6C_6(i,j+1)+C_{66}C_6(i+1,j+1)+C_{65}C_5(i,j+1)$$
$$+C_{63}C_3(i,j+1)=D_6C_6(i,j) \tag{5.18}$$

The meanings of all coefficients are explained as below:

We denote the space step and time step as $\triangle x=h$ and $\triangle t=k$.

$$\begin{aligned}
A_1 &= -\frac{a_1}{h^2}+\frac{b_1}{2h}, B_1=\frac{1}{k}+\frac{2a_1}{h^2}-c_{11}, C_{11}=-\frac{a_1}{h^2}-\frac{b_1}{2h}, C_{12}=-c_{12}, D_1=\frac{1}{k};\\
A_2 &= -\frac{a_2}{h^2}, B_2=\frac{1}{k}+\frac{2a_2}{h^2}+c_{22}, C_{22}=-\frac{a_2}{h^2}, C_{21}=-c_{21}, C_{23}=-c_{23}, D_2=\frac{1}{k};\\
A_3 &= -\frac{a_3}{h^2}, B_3=\frac{1}{k}+\frac{2a_3}{h^2}+c_{33}, C_{33}=-\frac{a_3}{h^2}, C_{32}=-c_{32}, D_3=\frac{1}{k};\\
A_4 &= -\frac{a_4}{h^2}+\frac{b_4}{2h}, B_4=\frac{1}{k}+\frac{2a_4}{h^2}-c_{41}, C_{44}=-\frac{a_4}{h^2}-\frac{b_4}{2h}, C_{45}=-c_{42}, D_4=\frac{1}{k};\\
A_5 &= -\frac{a_5}{h^2}, B_5=\frac{1}{k}+\frac{2a_5}{h^2}+c_{52}, C_{55}=-\frac{a_5}{h^2}, C_{54}=-c_{51}, C_{56}=-c_{53}, D_5=\frac{1}{k};\\
A_6 &= -\frac{a_6}{h^2}, B_6=\frac{1}{k}+\frac{2a_6}{h^2}+c_{63}, C_{66}=-\frac{a_6}{h^2}, C_{65}=-c_{62}, C_{63}=-c_{64}, D_6=\frac{1}{k}.
\end{aligned}$$

Now we use matrix called A to represent coefficients of above equations: see Fig.5.1. The corresponding linear system is represented as:

$$AC_{n+1} = C_n \tag{5.19}$$

Column-wise Gaussian Elimination method is applied to solve the linear systems. Six unknowns are solved. Comparing the numerical values of ${}^oC_{cap}$ to experimental data (Fig.4.2) oxygen consumption rate is adjusted.

5.2 Discussion about Numerical Scheme

The most basic property that a scheme must have in order to be useful is that its solutions approximate the solution of the corresponding partial differential equation and that the approximation improves as the grid spacings, h and k, tend to zero. We call such a scheme a *convergent scheme*. We need to judge the stability and convergency.

Here we apply the backward-time central-space scheme described as below:

$$\frac{u(m,n+1)-u(m,n)}{k} = b\frac{u(m+1,n+1)-2u(m,n+1)+u(m-1,n+1)}{h^2} \tag{5.20}$$

$$(-b\mu)u(m-1,n+1)+(1+2b\mu)u(m,n+1)+(-b\mu)u(m+1,n+1) = u(m,n)$$

We analyze the stability by replacing $u(m,n)$ by $g^n e^{im\theta}$, that is $u(m,n) = g^n e^{im\theta}$.

The amplification factor for the scheme satisfies

$$\begin{aligned}(-b\mu)ge^{-i\theta}+(1+2b\mu)g+(-b\mu)ge^{i\theta} &= 1\\ g &= \frac{1}{1+b\mu sin^2\frac{\theta}{2}}\end{aligned} \tag{5.21}$$

Figure 5.1: Coefficient Matrix

When $|g| \leq 1$, we have $b\mu > 0$. This scheme is implicit and unconditionally stable. It is accurate of order (1,2) and is dissipative when $b\mu > 0$. It can be shown by using Taylor Expansion that the scheme is also consistent.

At the same time we can use results of calculation to show the scheme is stable. Let C represents the oxygen concentration in capillary space, which comes from experimental data. C_n is the corresponding numerical value. n is the number of time steps. From the below table we can find $Min||C-C_n||$ decreases when n is increasing. That is reasonable because the error becomes smaller and smaller when we decrease the time step size. (see table 5.1)

n	$Min\|\|C - C_n\|\|$
100	0.1215
200	3.2798×10^{-4}
400	1.2789×10^{-7}
800	6.8692×10^{-12}

Table 5.1: Effection of Time Step Size

We also discuss mesh independence using table 5.2 (shown below) acquired by calculating $Min||C_{m_1,n} - C_{m_2,n}||$.

n	**Groups**	$Min\|\|C_{m_1,n} - C_{m_2,n}\|\|$
n=600	m=20,m=40	0.0784
	m=40,m=80	0.0384
	m=80,m=160	0.0190
n=1200	m=20,m=40	0.0785
	m=40,m=80	0.0385
	m=80,m=160	0.0190
n=2400	m=20,m=40	0.0785
	m=40,m=80	0.0385
	m=80,m=160	0.0191

Table 5.2: Effect of Space Step Size

Chapter 6

Results

In previous chapters we built the mathematical model and gave the numerical method for the model. Based on those mathematical model and numerical method we designed the corresponding algorithm. In this chapter we figure out the results of oxygen consumption rate (G) by fitting curve after given other parameters and furthermore analyze relationships between G and other parameters. Besides this we introduce the relationships between output and other parameters. In this chapter we continue to use the notations defined in previous chapters.

6.1 Determination of Oxygen Consumption Rate (G_{pc})

To test the behavior of the model, a single set of realistic parameter values was used as a starting point. This data set was in agreement with published data as well as with parameter values chosen to fit residue and the outflow dilution curves after injection of ^{15}O-labeled RBCs in an isolated heart preparation. Where values for a parameter were not available from the literature, known relationships to other

parameters were used to constrain this parameter value. The aim was to obtain fixed values for as many parameters as possible to minimize the degrees of freedom for exploring the behavior of the model and to fit the data obtained from tracer-dilution experiments after injection of $[^{15}O]$ oxygen [10].

The capillary length is taken to be $0.1cm$ [6]. We set the velocity of oxygen and water all as $0.3556cm \cdot min^{-1}$. Volume terms(V) describe oxygen and water volumes in three regions. Here we only consider efficient (virtual) volumes. See table 6.1 [6, 11, 34].

	${}^{o}V(ml/g)$	${}^{w}V(ml/g)$
Capillary, 70 Torr	0.07000	0.070
ISF, 60 Torr	0.00309	0.181
Parenchymal, 10 Torr	0.05870	0.544

Table 6.1: Volume parameters for representative conditions with a Hct of 0.2 and arterial PO_2 of 100 Torr

Dispersion terms (D) describe the axial dispersion of oxygen and water. The unit is $cm^2 \cdot s^{-1}$. The overall diffusion coefficients using the approach of [31] accounts for diffusion in series and in parallel and for permeation on all erythrocyte surfaces.

For oxygen

${}^{o}D_{cap} = 1.67 \times 10^{-5}$ [31],${}^{o}D_{isf} = 0.092 \times 10^{-5}$ [10],${}^{o}D_{pc} = 1.16 \times 10^{-5}$ [19, 16].

For water

${}^{w}D_{cap} = 1.36 \times 10^{-5}$ [26],${}^{w}D_{isf} = 0.52 \times 10^{-5}$ [31],${}^{w}D_{pc} = 0.66 \times 10^{-5}$ [31].

Conductant terms(PS) describe the resistance forces between two barriers.

For oxygen

${}^{o}PS_{cap} = 0.4$,${}^{o}PS_{pc} = 5$ [10].

For water

${}^wPS_{cap} = 7, {}^wPS_{pc} = 0.6$ [10].

G_{pc} is the oxygen metabolic clearance, which is assumed 1.0 $ml \cdot g^{-1} \cdot min^{-1}$. After adjusting G_{pc} we get the Fig.6.1. $*$ represents the experimental inflow data. We use natural cubic spline algorithm to interpolate the data. $\circ$ represents the experimental outflow (oxygen+water) data. Solving PDEs we calculate oxygen outflow and water outflow in capillary.

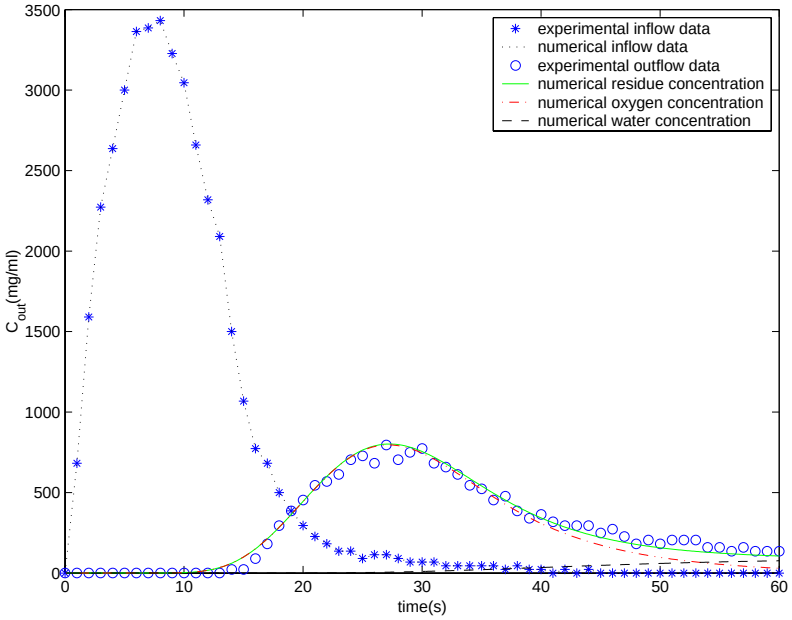

Figure 6.1: Numerical Result Compare to Experimental Data

G_{pc} was calculated by fitting curve which is 0.42. As we stated in previous chapters, the most direct measure of oxidative tissue metabolism is oxygen consumption rate. Although at present the experiments are made for animals, it has deep meaning for human being in future. In Fig.6.2 the outflow data from experiments match residue concentration (oxygen+water) from numerical calculation.

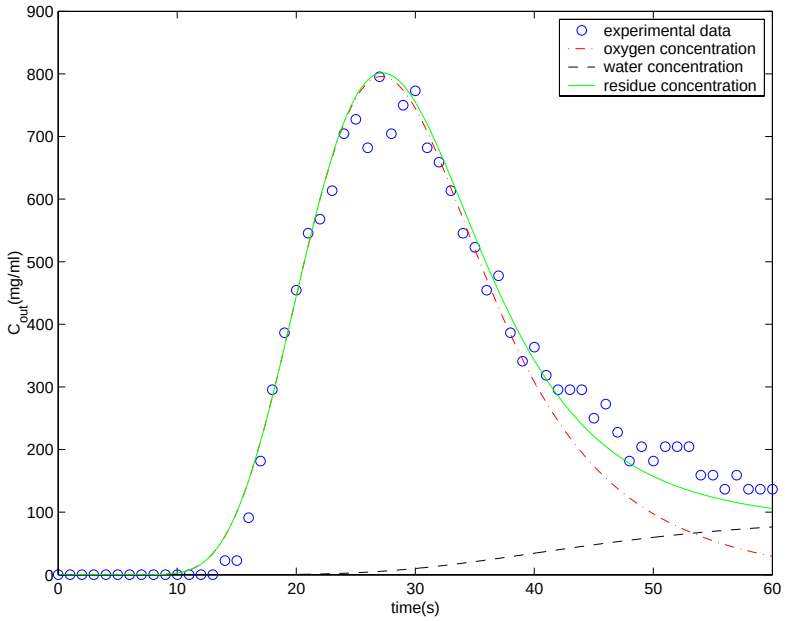

Figure 6.2: Numerical Results Match Experimental Outflow Data

6.2 Effects of Other Parameters on Oxygen Consumption Rate

6.2.1 Effects of Outflow Data on Oxygen Consumption Rate

After fixing other parameters and select the reasonable range of oxygen consumption rate (G_{pc}), we find there exists relationship between concentration (oxygen, water and residue in capillary) and oxygen consumption rate (G). When oxygen concentration ($^oC_{cap}$) are increased, G decreases. Fig.6.2. with G on the vertical axis and $^oC_{cap}$ on the horizontal axis show this point. In contrast, when water concentration ($^wC_{cap}$) are increased, G increases. The trend can be seen from Fig.6.3. The joint effect of oxygen and water is that when residue increases, G_{pc} decreases. See Fig.6.4.

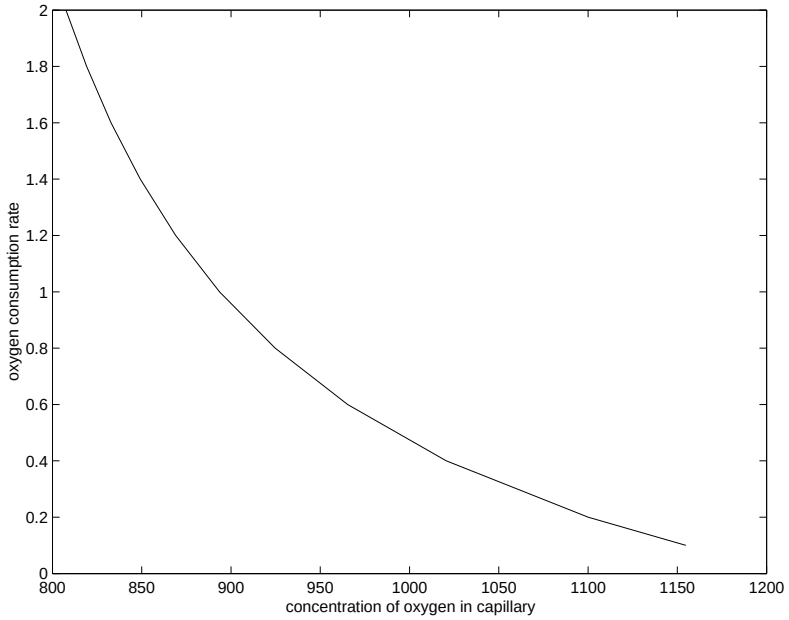

Figure 6.3: When oxygen concentration increases, G_{pc} decreases

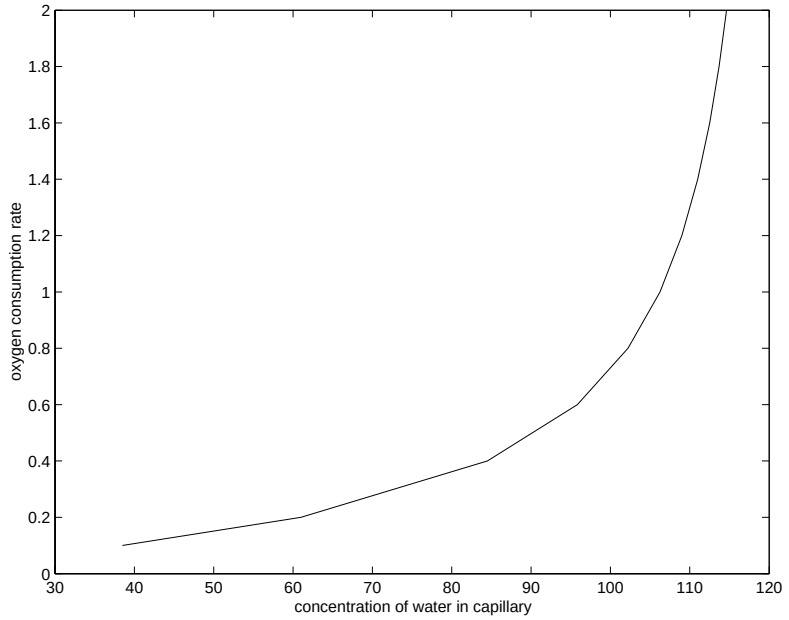

Figure 6.4: When water concentration increases, G_{pc} decreases

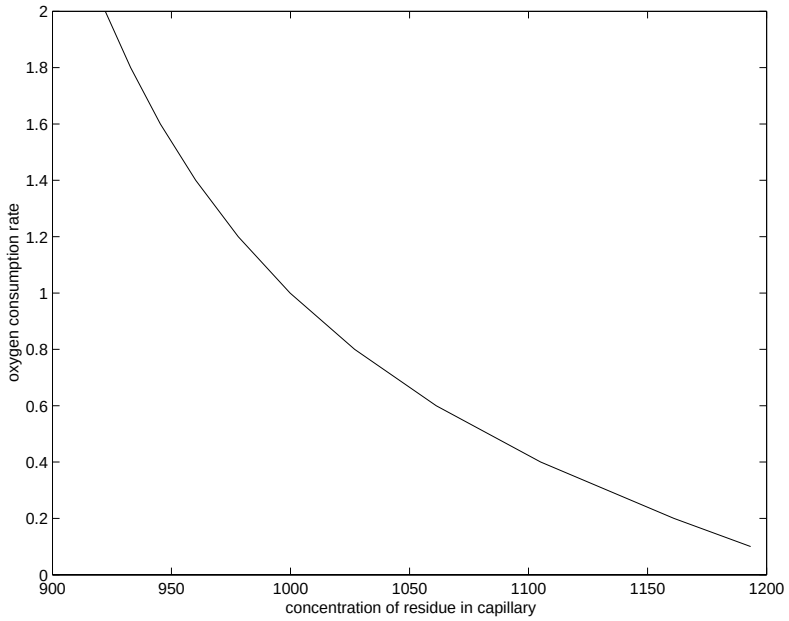

Figure 6.5: When outflow residue increases, G_{pc} increases

6.2.2 Effects of Conductance on Oxygen Consumption Rate

After fixing other parameters and select the reasonable range of ${}^{o}PS_{cap}$,${}^{o}PS_{pc}$,${}^{w}PS_{cap}$ and ${}^{w}PS_{pc}$, we find there exists relationship between conductance parameters and oxygen consumption rate (G). When ${}^{o}PS_{cap}$,${}^{o}PS_{pc}$ are increased, G decreases. Fig.6.5 and Fig.6.6. with G on the vertical axis and ${}^{o}PS_{cap}$,${}^{o}PS_{pc}$ on the horizontal axis show this point. In contrast, when ${}^{w}PS_{cap}$,${}^{w}PS_{pc}$ are increased, G increases. The trend can be seen from Fig.6.7 and Fig.6.8.

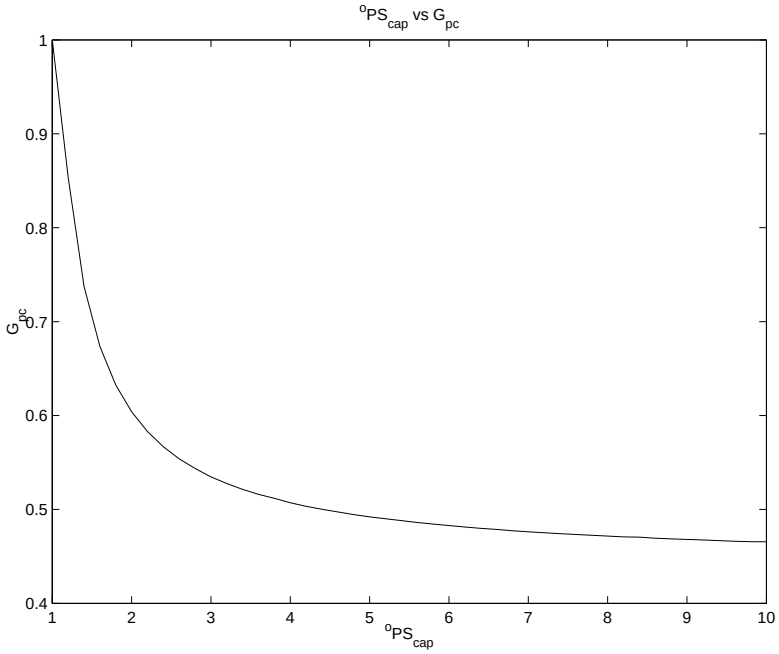

Figure 6.6: When ${}^oPS_{cap}$ increases, G_{pc} decreases

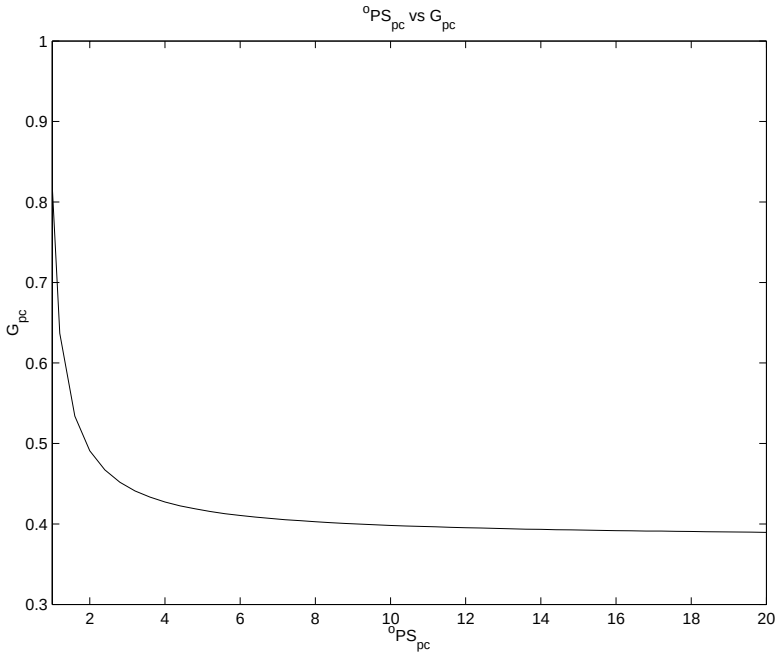

Figure 6.7: When ${}^oPS_{pc}$ increases, G_{pc} decreases

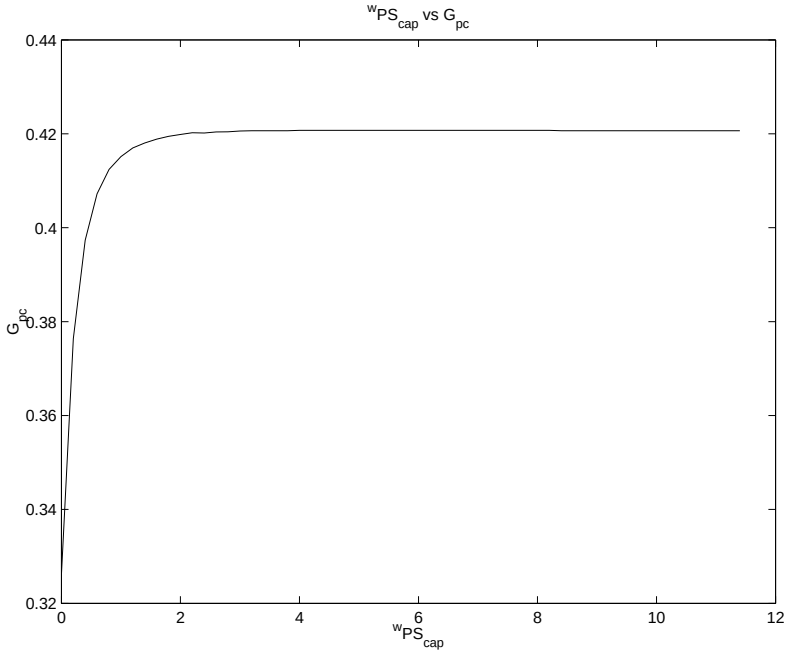

Figure 6.8: When ${}^{w}PS_{cap}$ increases, G_{pc} increases

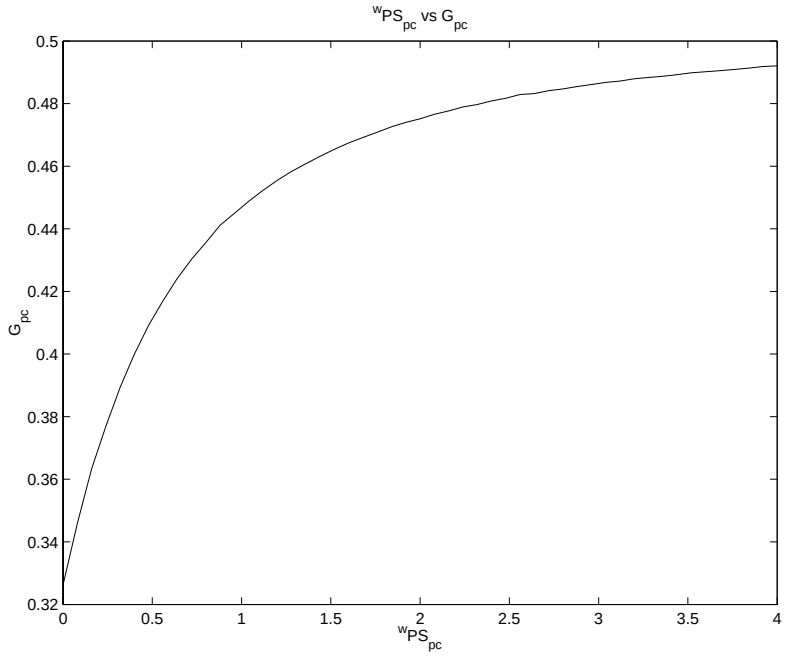

Figure 6.9: When ${}^{w}PS_{pc}$ increases, G_{pc} increases

6.2.3 Effects of Diffusion Coefficients and Velocity on Oxygen Consumption Rate

Diffusion parameters (${}^{o}D_{cap}, {}^{o}D_{isf}, {}^{o}D_{pc}, {}^{w}D_{cap}, {}^{w}D_{isf}, {}^{w}D_{pc}$) have little effects on oxygen consumption rate. Here we do not discuss them any more.

Oxygen consumption rate increases when velocity parameters (${}^{o}v, {}^{w}v$) increase (see Fig.6.9). However, if the range of local flows is broad, then the error will be greater [10].

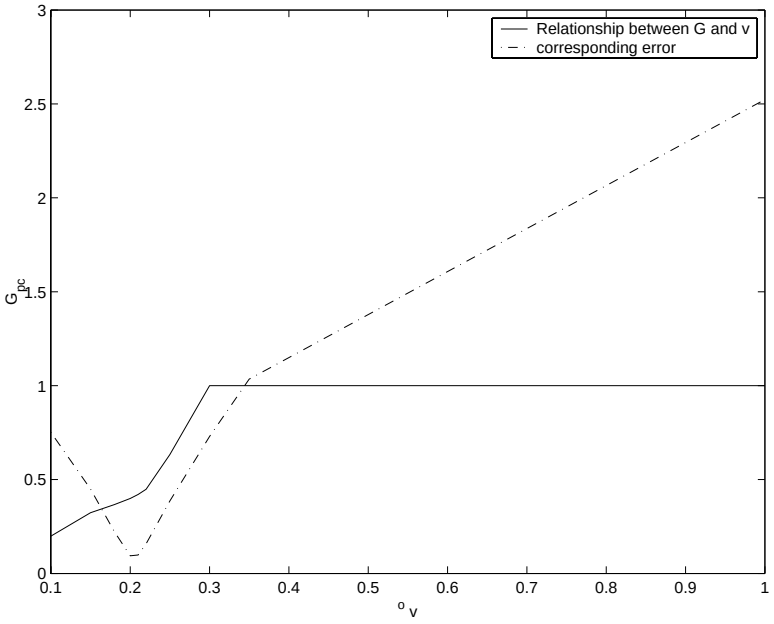

Figure 6.10: When velocity increases, G_{pc} increases

6.3 Effects of Parameters on Outflow

6.3.1 Oxygen Conversion Rate(G) Effects on Residue Concentration (Outflow Data)

If increasing oxygen conversion rate, metabolism will speed up. There will be more oxygen transfering to water. So Fig.6.10 shows this procedure. At the same time the amount of water will increase (see Fig.6.11). The whole residue will show the final results (see Fig.6.12). At the last stage oxygen and water residue will stabilize as one level.

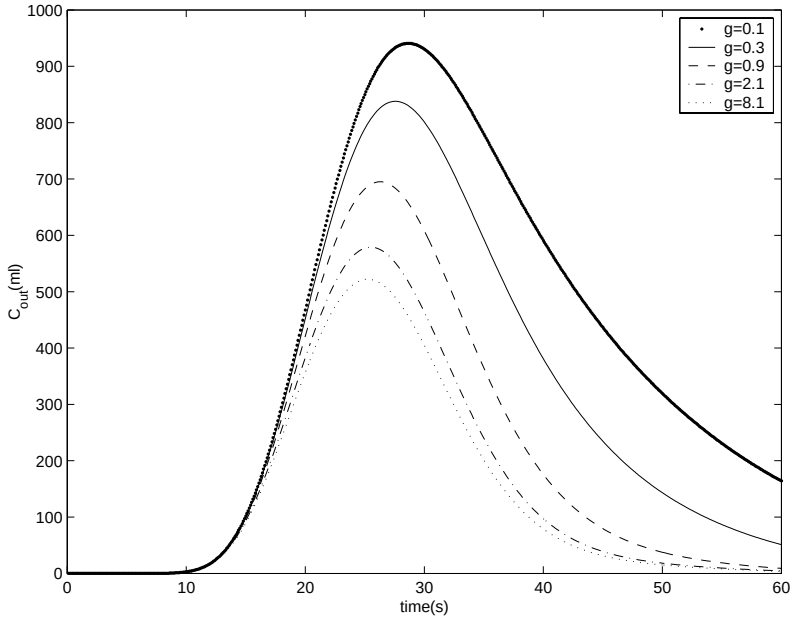

Figure 6.11: G_{pc} increases the change rate of Oxygen Residue Concentration in Capillary

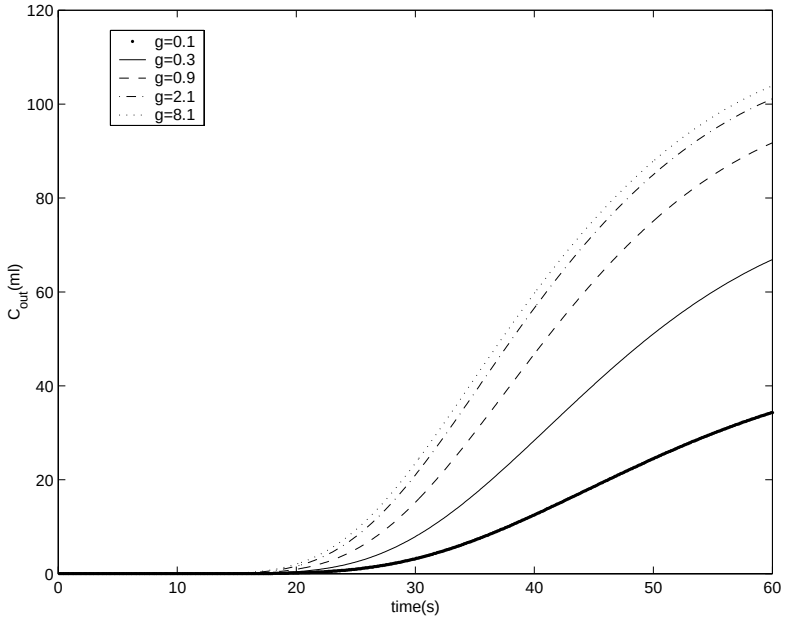

Figure 6.12: G_{pc} increases the change rate of Water Residue Concentration in Capillary

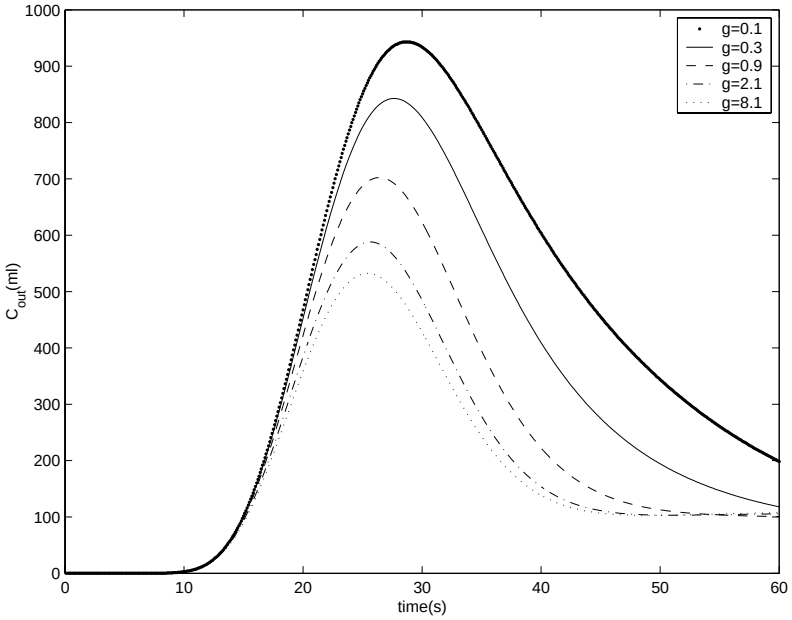

Figure 6.13: G_{pc} increases the change rate of Residue(Oxygen+Water) Concentration in Capillary

6.3.2 Velocity(^{o}v) Effects on Residue Concentration

When we increase the velocity of oxygen in capillary, the metabolism will happen earlier. So from the picture we can see oxygen residue concentration became higher when velocity was increased. And water residue concentration also became higher. The results can be seen in Fig.6.13 and Fig.6.14. The joint effect is that oxygen concentration decreases when velocity increases (see Fig.6.15).

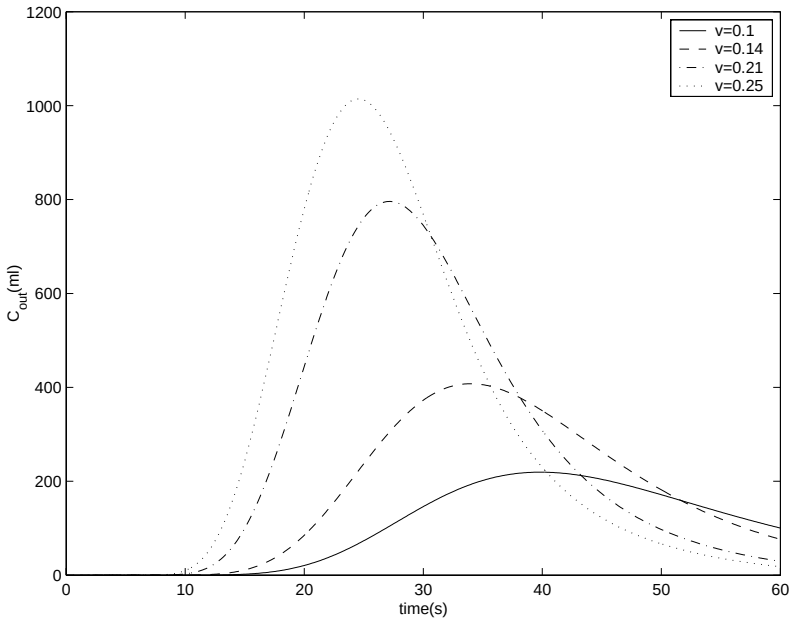

Figure 6.14: Velocity Increases Oxygen Residue Concentration in Capillary

6.3.3 Conductance Coefficients Effects on Residue Concentration

Fig.6.16 and Fig.6.17 show $^{o}PS_{cap}$ effects on the concentration of oxygen and water residue in capillary vessel. It is easily seen that $^{o}PS_{cap}$ has a significant impact on the concentrations. When $^{o}PS_{cap}$ increases, there are more oxygen passing

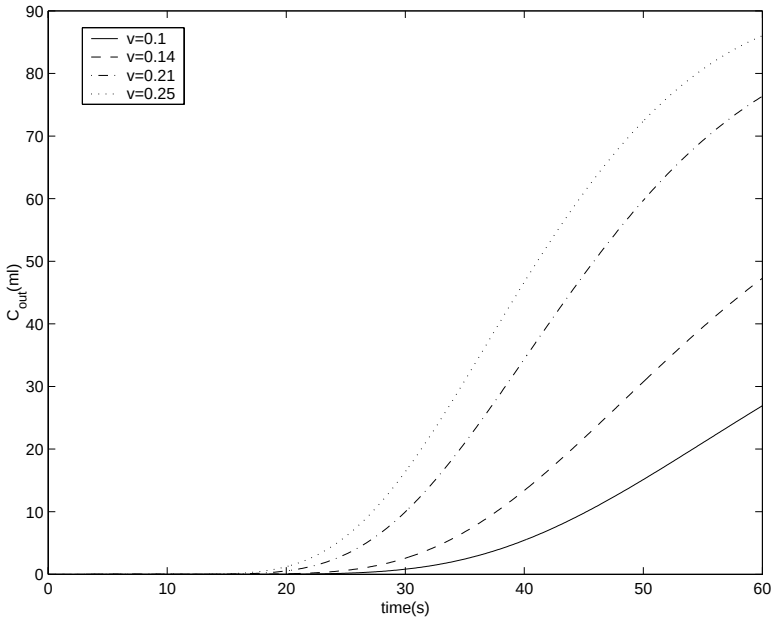

Figure 6.15: Velocity Increases Water Residue Concentration in Capillary

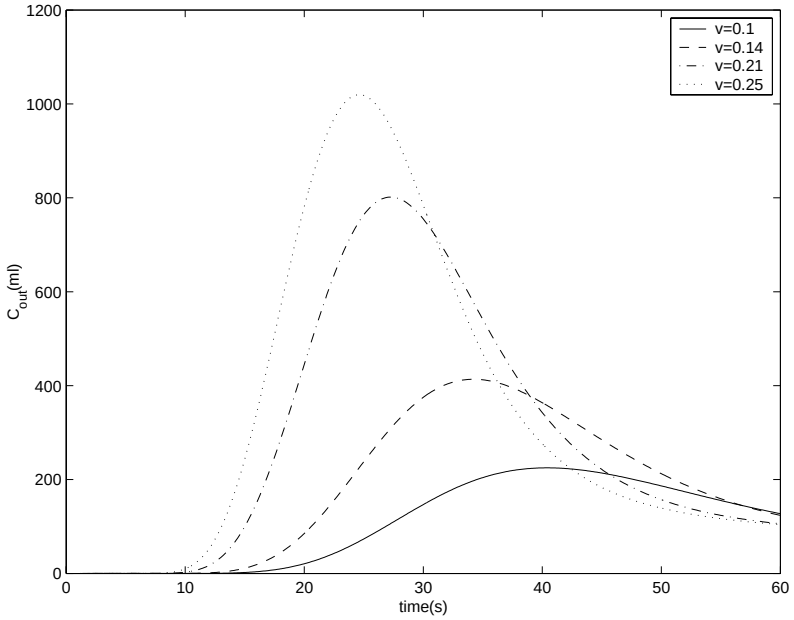

Figure 6.16: Velocity Increases Residue(Oxygen+Water) Concentration in Capillary

through capillary-interstitial membrane to interstitial part (see Fig.6.16). Oxygen concentration changes fast because the oxygen extraction increases.

${}^{o}PS_{cap}$ has only small effects water residue. From the result water residue concentration decreases slightly when oxygen extraction increases (see Fig.6.17). This is because oxygen extraction between different membranes increases and the metabolism part reduces. Effects on whole residue (Oxygen+Water) mainly comes from effects on oxgyen. So they reduce when ${}^{o}PS_{cap}$ increases (see Fig.6.18).

${}^{o}PS_{pc}$ does not have as obvious effects as ${}^{o}PS_{cap}$ because ${}^{o}PS_{pc}$ is oxygen extraction between interstitial and parenchymal membranes (see Fig.6.19). But it has a bigger effects on oxygen in parenchymal part.

${}^{w}PS_{cap}$ affects concentration of oxygen and water residue slightly, especially oxygen residue. The pictures are not shown.

${}^{w}PS_{pc}$ affects oxygen residue slightly. But it accelerates the outflow of water (see Fig.6.20). When time is $60s$, $PS = 0.1$ corresponds concentration of oxygen residue $92ml$; $PS = 0.6$, concentration is $76ml$; $PS = 2.7$, concentration is $26ml$. Effects on whole residue (Oxygen+Water) mainly come from effects on water (see Fig.6.21).

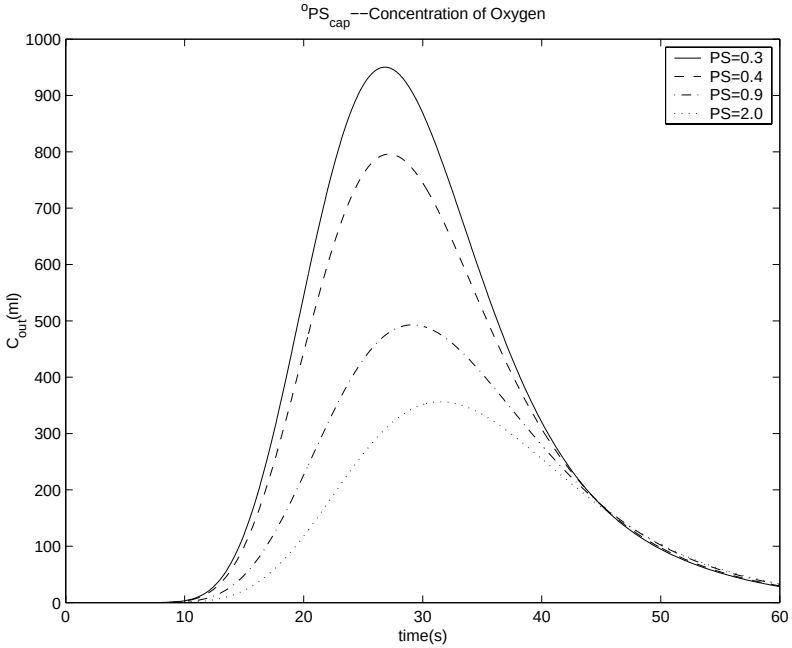

Figure 6.17: ${}^{o}PS_{cap}$ Decreases Concentration of Oxygen Residue in Capillary

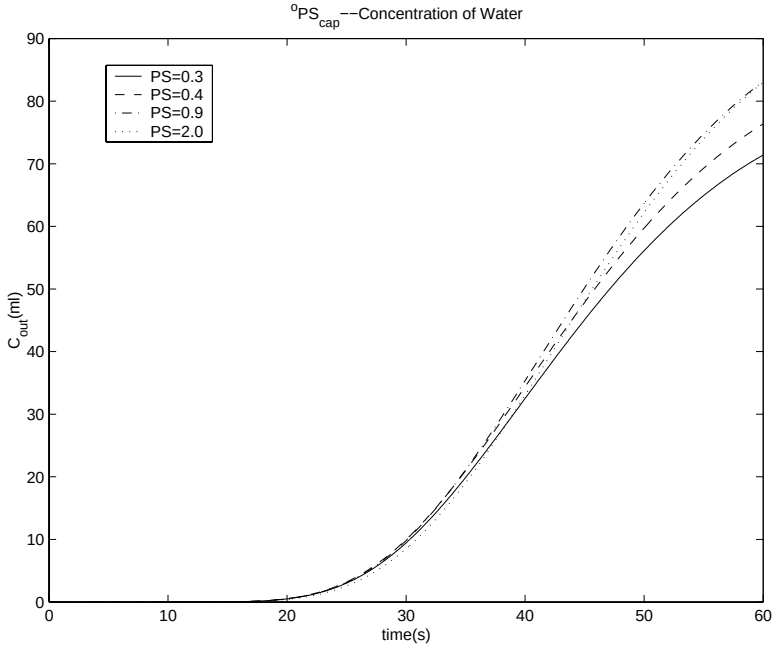

Figure 6.18: ${}^{o}PS_{cap}$ Increases Concentration of Water Residue in Capillary

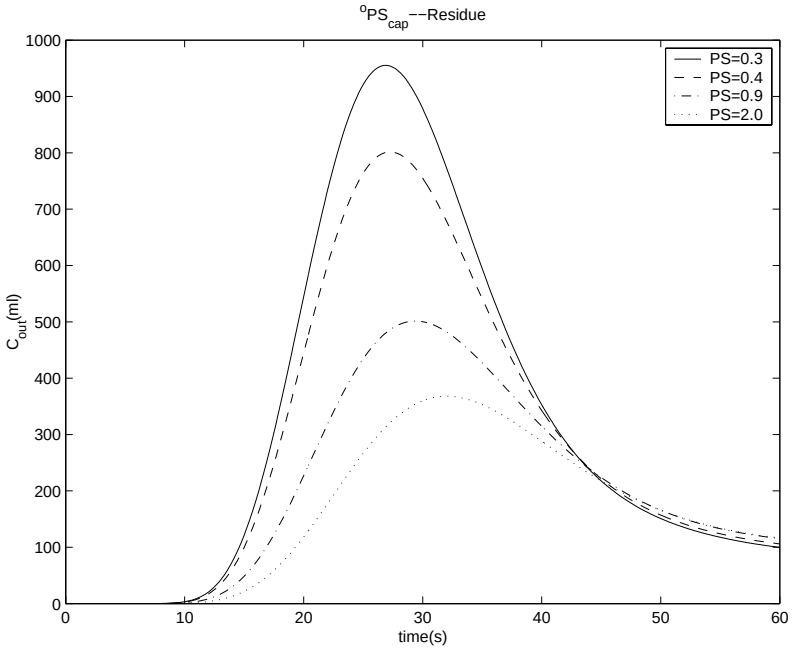

Figure 6.19: ${}^{o}PS_{cap}$ Decreases Residue (Oxygen+Water) in Capillary

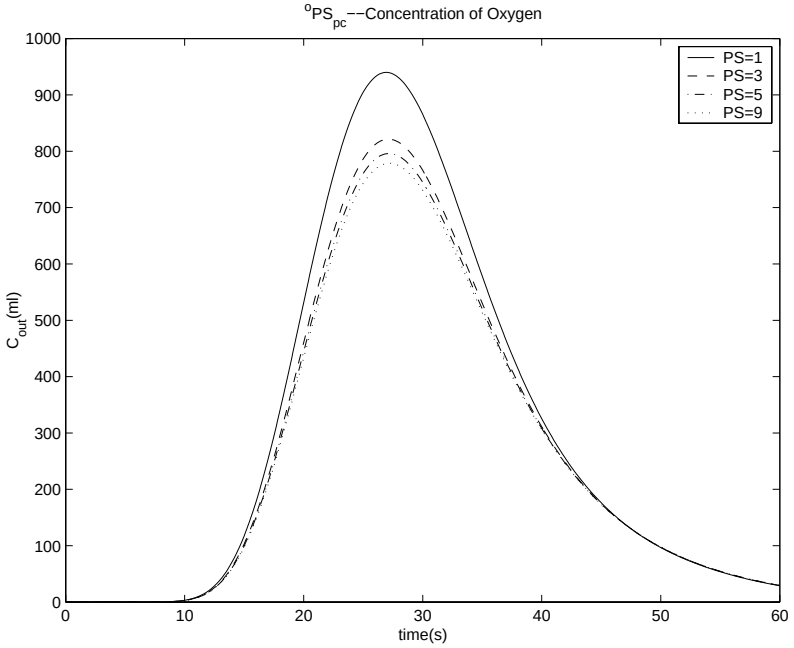

Figure 6.20: ${}^{o}PS_{pc}$ Decreases Concentration of Oxygen Residue in Capillary

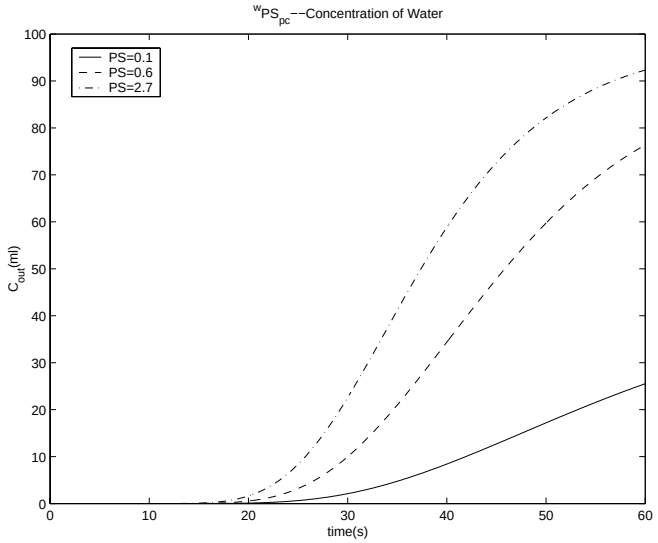

Figure 6.21: ${}^{w}PS_{pc}$ Increases Concentration of Water Residue in Capillary

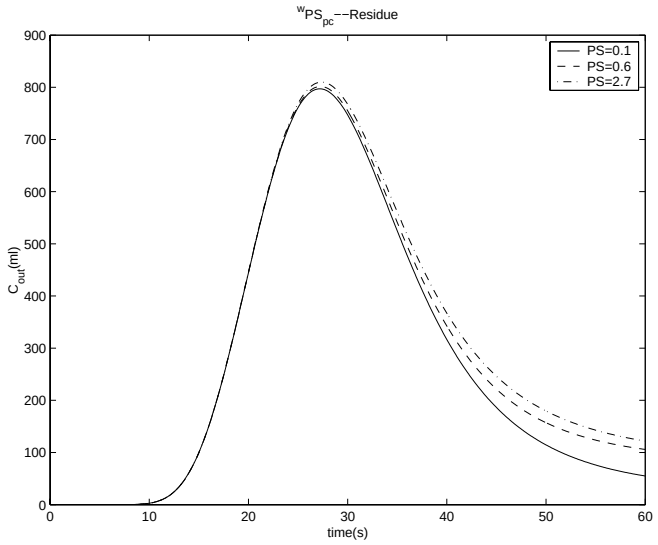

Figure 6.22: ${}^{w}PS_{pc}$ Increases Residue (Oxygen+Water) in Capillary

6.3.4 Diffusion Coefficients Effects on Residue Concentration

Fig.6.22 shows that when diffusion coefficient ${}^{o}D_{cap}$ increases, the whole oxygen residue concentration moves to left. That is because metabolism happens early. Oxygen conversion procedure comes early. But the change is not obvious. ${}^{o}D_{cap} = 1.0 \times 10^{-4}$ does not make sense. Also from the Fig 6.23 when diffusion coefficient ${}^{o}D_{cap}$ increases, the whole water residue concentration moves to left too.

${}^{o}D_{isf}$ has small effects on oxygen residue concentration. ${}^{o}D_{isf}$ decreases the concentration of oxygen and increases the concentration of water (see Fig.6.25 and Fig.6.26). Because the diffusion increases, the whole metabolism speeds up (see Fig.6.27).

But here some high values (10^{-4}) and very high values (10^{-2}) are tried. They will lower the peak of oxygen residue concentration in capillary and flatten water residue concentration. In fact the interstitium becomes in effect a uniform mixing chamber. These values are inappropriate and seriouly distort the curve shapes [10].

${}^{w}D_{cap}$ has slight effects on oxygen residue concentration, which is not shown. When ${}^{w}D_{cap}$ increases, it flattens water residue concentration (see Fig.6.28). It shows that the water concentration increases when ${}^{w}D_{cap}$ increases. From the picture of effects on residue the whole curve becomes sharpen (see Fig.6.29). The effect of water is bigger than that of oxygen. But the change is not obvious.

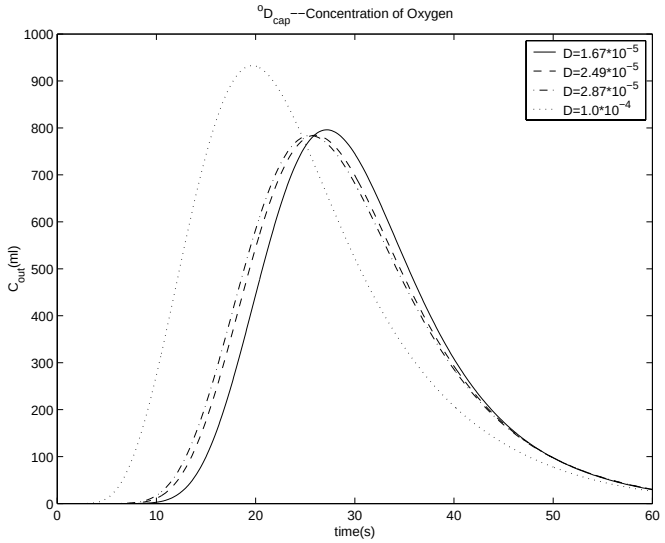

Figure 6.23: When $^oD_{cap}$ increases, oxygen consumption will happen early

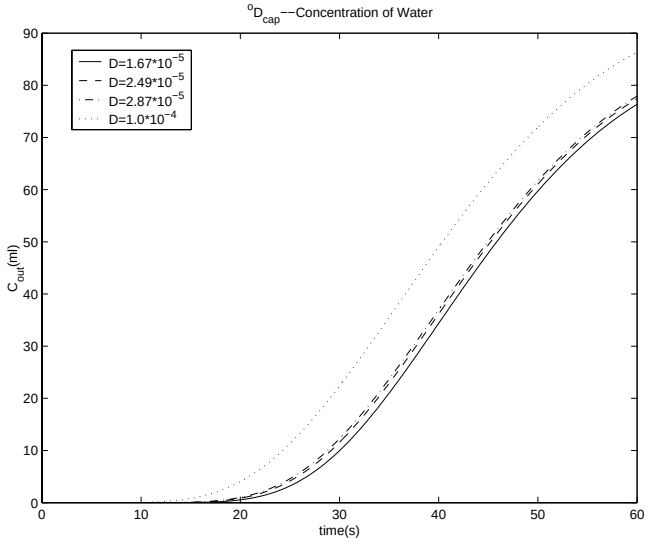

Figure 6.24: When $^oD_{cap}$ increases, water production will happen early

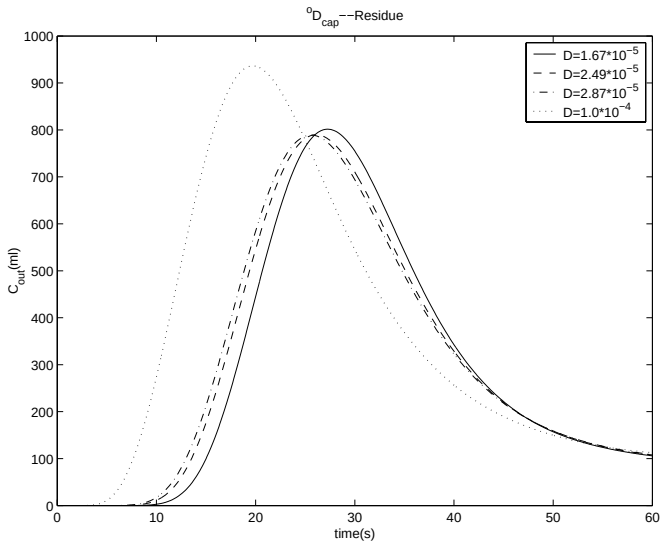

Figure 6.25: When $^oD_{cap}$ increases, metabolism procedure will happen early

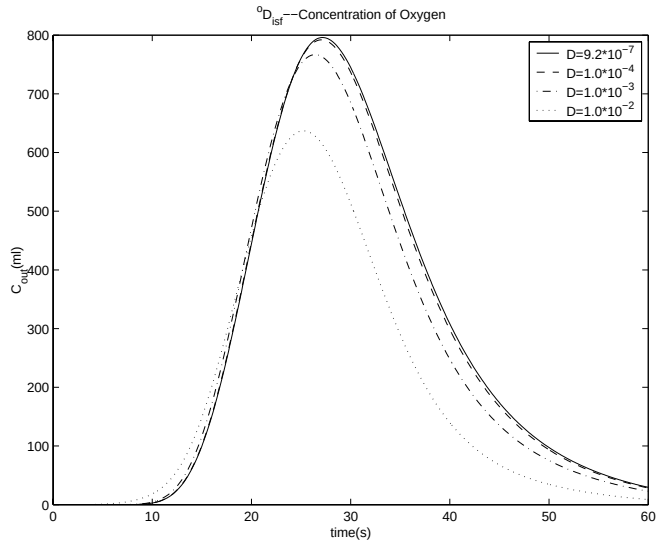

Figure 6.26: $^oD_{isf}$ decreases the oxygen concentration in capillary

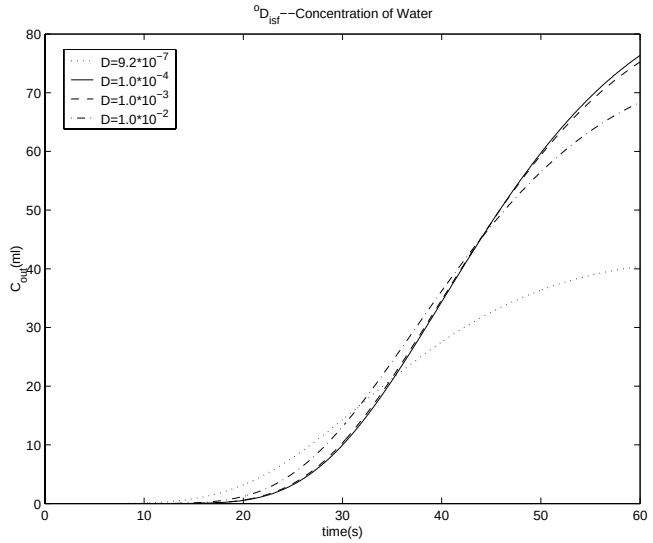

Figure 6.27: ${}^{o}D_{isf}$ increases the water concentration in capillary

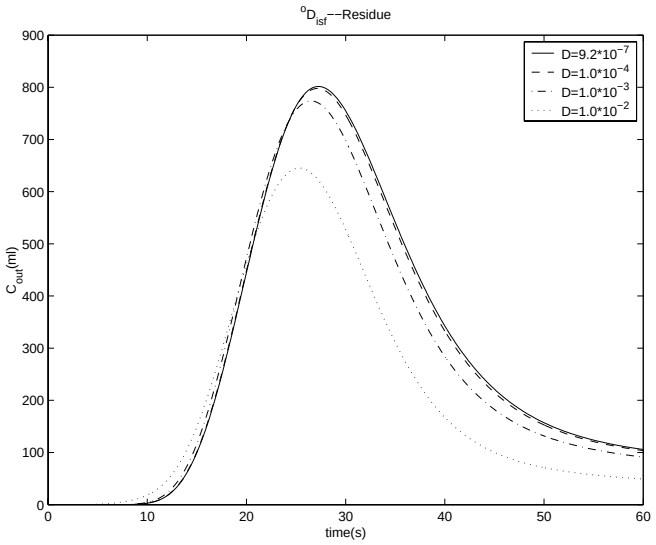

Figure 6.28: ${}^{o}D_{isf}$ accelerates the consumption procedure

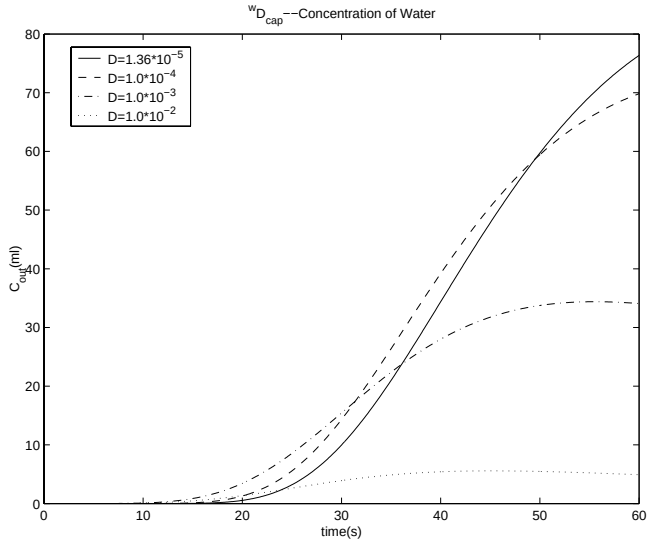

Figure 6.29: ${}^{w}D_{cap}$ decreases the water concentration in capillary

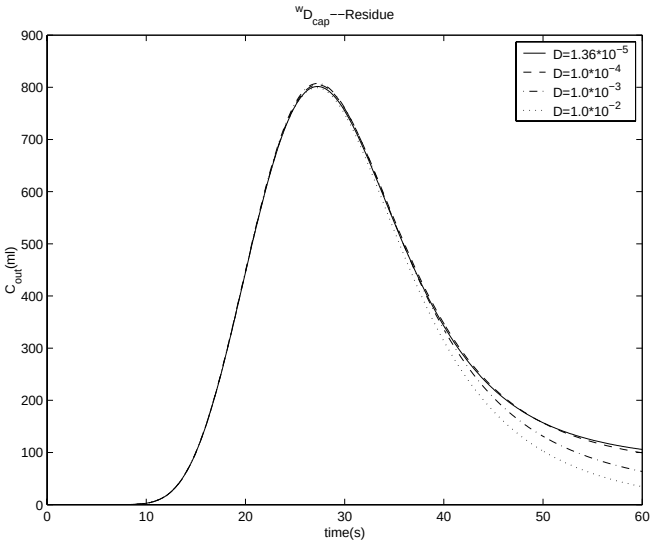

Figure 6.30: ${}^{w}D_{cap}$ shows subtle effects on residue in capillary

Chapter 7

Conclusion

The most direct measure of oxidative tissue metabolism is the conversion rate of oxygen to water. Oxygen consumption rate is an important parameter to measure if heart muscle is working well. Our research in medical field is very meaningful. Based on mass conservation we develop the blood-tissue model which is three-region axially distributed. The objective of our model is to find such an oxygen consumption rate that experimental outflow data matches numerical data.

Using fitting curve method we found the oxygen consumption rate. The numerical method is simple and the computational speed is considerable. We also discuss the relationship between oxygen consumption rate and other parameters. 1) When oxygen concentration in capillary increases, oxygen consumption rate decreases. 2) When oxygen conductances increase, oxygen consumption rate decreases. 3) When water conductances increase, oxygen consumption rate increases. 4) Diffusion parameters have little effects on oxygen consumption rate. 5) Oxygen consumption rate increases when velocity parameters increase. However, if the range of local flows is broad, the error will be greater.

Bibliography

[1] Benefits of PET Exams Homepage: `http://www.allianceimaging.com`, 2000.

[2] King R. B., J. B. Bassingthwaighte, J. R. S. Hales, and L. B. Rowell. Stability of heterogeneity of myocardial blood flow in normal awake baboons. *Circ. Res.57*, pages 285–295, 1985.

[3] J.B. Bassingthwaighte. Plasma indicator dispersion in arteries of the human leg. *Circ. Res.19*, pages 332–346, 1966.

[4] J.B. Bassingthwaighte. A concurrent flow model for extraction during transcapillary passage. *Circ. Res 35*, pages 483–503, 1974.

[5] J.B. Bassingthwaighte, I.S. Joseph Chan, and C.Y. Wang. Computationally efficient algorithms for convection-permeation-diffusion models for blood-tissue exchange. *Annals of Biomedical Engineering, Vol. 20*, pages 688–689, 1992.

[6] J.B. Bassingthwaighte, T. Yipintsoi, and R.B. Harvey. Microvasculature of the dog left ventricular myocardium. *Microvasc. Res.*, pages 229–249, 1974.

[7] A.J. Chorin and J.E. Marsden. *A Mathematical Introduction to Fluid Mechanics*. Springer-Verlag New York Inc., 1979.

[8] A compartmental model tutorial Homepage: `http://depts.washington.edu/rfpk/training/tutorials/modeling/part1/20.html`, 2002.

[9] John Crank. *The Mathematics of Diffusion.* Oxford Clarendon Press, 1956.

[10] Andreas Deussen and James B. Bassingthwaighte. Modeling $[^{15}o]$ oxygen tracer data for estimating oxygen consumption, 1996.

[11] F. Gonzalez and J.B. Bassingthwaighte. Heterogeneities in regional volumes of distribution and flows in the rabbit heart. *Am. J. Physiol. 258*, pages H1012–H1024, 1990.

[12] C.A. Goresky, W.H. Ziegler, and G.G. Bach. Capillary exchange modeling: Barrier-limited and flow-limited distribution. *Circ. Res 27*, pages 739–764, 1970.

[13] B. Guller, T. Yipintsoi, A. L. Orvis, and J. B. Bassingthwaighte. Myocardial sodium extraction at varied coronary flows in the dog: estimation of capillary permeability by residue and outflow detection. *Circ. Res.37*, pages 359–378, 1975.

[14] The Columbia University College of Physicians and Surgeons Homepage: `http://cpmcnet.columbia.edu/texts/guide/hmg16_0003.html#16.8`, 2002.

[15] The Columbia University College of Physicians and Surgeons Homepage: `http://cpmcnet.columbia.edu/texts/guide/toc/toc16.html`, 2002.

[16] L.D. Homer, J.B. Shelton, C.H. Dorsey, and T.J. Williams. Anisotropic diffusion of oxygen in slices of rat muscle. *Am. J. Physiol. 246*, pages R107–R113, 1984.

[17] Groebe K. A versatile model of steady state o_2 supply to tissue. application to skeletal muscle. *Biophys J 1990 Mar;57(3)*, pages 485–398, 1990.

[18] Hristo V. Kojouharov and Benito M. Chen. *Nonstandard Methods for Advection-Diffusion-Reaction Equations.* World Scientific, 1999.

[19] L. De Koning, J.C. Hoofd, and F. Kreuzer. Oxygen transport and the function of myoglobin: Theoretical model and experiments in chicken gizzard smooth muscle. *Pfluegers Arch. 389*, pages 211–217, 1981.

[20] A.M. Lenhoff and E.N. Lightfoot. The effects of axial diffusion and permeability barriers on the transient response of tissue cylinders. ii. solution in time domain. *J. Theor. Biol. 106*, pages 207–238, 1984.

[21] C.J. Lumsden and M. Silverman. Exchange of multiple multiple indicators across renal-like epithelia: A modeling study of six physiological regimes. *Am. J. Physiol. 25*, pages F1073–F1089, 1986.

[22] J. Mazziotta, S. Gilman, and Eds. Clinical brain imaging: Principles and applications. F.A. Davis Company, 1992.

[23] Secomb TW McGuire BJ. A theoretical model for oxygen transport in skeletal muscle under conditions of high oxygen demand. *J Appl Physiol 2001 Nov;91(5)*, pages 2255–65, 2001.

[24] http://www.austin.unimelb.edu.au/dept/nmpet/detail/clinical.html, 2000.

[25] http://www.austin.unimelb.edu.au/dept/nmpet/pet/detail/principle.html, 2000.

[26] W. R. Redwood, E. Rall, and W. Perl. Red cell membrane permeability deduced from bulk diffusion coefficients. *J. Gen. Physiol. 64*, pages 706–729, 1974.

[27] Wiesner R.J., A. Deussen, M. Borst, J. Schrader, and M.K. Grieshaber. Glutamate degradation in the ischemic dog heart: contribution to anaerobic energy production. *J. Mol. Cell. Cardiol. 21*, pages 49–59, 1989.

[28] C.P. Rose, C.A. Goresky, and G.G. Bach. The capillary and sarcolemmal barriers in the heart: An exploration of labeled water permeability. *Circ. Res 41*, pages 515–533, 1976.

[29] Goresky CA Rose CP. Limitations of tracer oxygen uptake in the canine coronary circulation. *Circ Res 1985 Jan;56(1)*, pages 57–71, 1985.

[30] Napper SA and Schubert RW. Mathematical evidence for flow-induced changes in myocardial oxygen consumption. *Ann Biomed Eng 1988;16(4)*, pages 349–365, 1988.

[31] R.E. Safford, E.A. Bassingthwaighte, and J.B. Bassingthwaighte. Diffusion of water in cat ventricular myocardium. *J. Gen. Physiol. 72*, pages 513–538, 1978.

[32] A.C. Sangren and C.W. Sheppard. A mathematical derivation of the exchange of a labeled substance between a liquid flowing in a vessel and an external compartment. *Bull.Math.Biophys. 15*, pages 387–394, 1953.

[33] Graham B. Wallis. *One-dimensional Two-phase Flow*. McGraw-Hill Book Company, 1969.

[34] T. Yipintsoi, P.D. Scanlon, and J.B. Bassingthwaighte. Density and water content of dog ventricular myocardium. *Proc. Soc. Exp. Biol. Med. 141*, pages 1032–1035, 1972.